University of Minnesota

Hypersonic Aerodynamics
AEM 4247/5247

Spring Semester 2022

Graham Candler
candler@umn.edu

Revision: January 20, 2022

I. Review of Compressible Gas Dynamics and Thermodynamics

Normal Shock Waves in Perfect Gases

Consider the flow from left to right with a shock wave perpendicular to the supersonic free-stream:

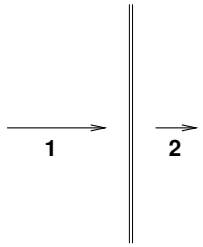

The one-dimensional conservation equations for a stationary shock wave are given by:

$$\rho_1 u_1 = \rho_2 u_2$$
$$\rho_1 u_1^2 + p_1 = \rho_2 u_2^2 + p_2$$
$$(E_1 + p_1)u_1 = (E_2 + p_2)u_2$$

where ρ is the density, u is the velocity, p is the pressure, and E is the energy of the gas per unit volume. We can write E as the sum of the internal energy and kinetic energy:

$$E = \rho e + \tfrac{1}{2}\rho u^2$$

where e is the internal energy per unit mass. It is convenient to use the specific enthalpy, h, which is related to the energy through:

$$h = e + p/\rho$$

Assuming a thermally perfect gas, the pressure is given by:

$$p = \rho R T$$

where R is the gas constant, and T is the temperature. In the thermally perfect case, we have $h = e + RT$.

Now consider the energy conservation equation above; we can combine the energy and pressure, and use the mass conservation equation to obtain a simple conservation law for the one-dimensional shock flow.

$$\rho_1 u_1 \big(e_1 + \tfrac{1}{2}u_1^2 + p_1/\rho_1\big) = \rho_2 u_2 \big(e_2 + \tfrac{1}{2}u_2^2 + p_2/\rho_1\big)$$
$$h_1 + \tfrac{1}{2}u_1^2 = h_2 + \tfrac{1}{2}u_2^2$$
$$h_{o1} = h_{o2}$$

where $h_o = h + \frac{1}{2}u^2$ is the total (or stagnation) enthalpy. Therefore, the total enthalpy is a conserved quantity across shock waves (and all for all adiabatic flows, where there is no heat addition or loss).

If the gas internal energy varies linearly with temperature, the gas is calorically perfect, and we can derive closed-form solutions to the normal shock wave flow. In this case, the internal energy is given by

$$e = c_v T$$

where c_v is the specific heat at constant volume, and is a constant. Similarly, the enthalpy is proportional to temperature:

$$h = c_p T = (c_v + R)T$$

where c_p is the specific heat at constant pressure. For the case of a thermally and calorically perfect gas, it is convenient to define γ as the ratio of specific heats:

$$\gamma = \frac{c_p}{c_v} = 1 + \frac{R}{c_v}$$

For most hypersonic applications, the gas is not calorically perfect and γ is not particularly useful.

For the time being, let us define the speed of sound of the gas, a, as:

$$a = \sqrt{\gamma RT} = \sqrt{\gamma \frac{p}{\rho}}$$

and the Mach number as:

$$M = \frac{|u|}{a}$$

Note that the square of the Mach number is proportional to the ratio of the kinetic energy to the internal energy. If we use this fact and assume a calorically perfect gas, we can rewrite the one-dimensional energy equation as:

$$\frac{T_2}{T_1} = \frac{1 + \frac{\gamma-1}{2}M_1^2}{1 + \frac{\gamma-1}{2}M_2^2}$$

Now using the mass conservation equation and the expression for the speed of sound, we obtain the pressure ratio across the shock wave as:

$$\frac{p_2}{p_1} = \frac{M_1}{M_2}\left(\frac{1 + \frac{\gamma-1}{2}M_1^2}{1 + \frac{\gamma-1}{2}M_2^2}\right)^{1/2}$$

The momentum equation can be written in terms of Mach number:

$$\frac{p_2}{p_1} = \frac{1+\gamma M_1^2}{1+\gamma M_2^2}$$

Now we have two equations for the pressure ratio, which allows us to solve for the post-shock Mach number as:

$$M_2 = \left(\frac{M_1^2 + \frac{2}{\gamma-1}}{\frac{2\gamma}{\gamma-1} M_1^2 - 1} \right)^{1/2}$$

This expression is only valid for $M_1 > 1$ and results in $M_2 < 1$. Thus, a shock wave converts upstream directed kinetic energy into internal energy as the gas goes from supersonic to subsonic flow.

We can now use the expressions above to obtain the pressure, density and temperature ratios across the shock wave:

$$\begin{aligned}
\frac{T_2}{T_1} &= \left(\frac{2\gamma}{\gamma+1} M_1^2 - \frac{\gamma-1}{\gamma+1} \right) \left(\frac{2}{(\gamma+1)M_1^2} + \frac{\gamma-1}{\gamma+1} \right) \\
\frac{\rho_2}{\rho_1} &= \frac{u_1}{u_2} = \frac{(\gamma+1)M_1^2}{2+(\gamma-1)M_1^2} \\
\frac{p_2}{p_1} &= \frac{2\gamma}{\gamma+1} M_1^2 - \frac{\gamma-1}{\gamma+1}
\end{aligned}$$

Speed of Sound in a Perfect Gas

The speed of sound is a thermodynamic quantity and is defined as the square root of the rate of change of pressure with respect to density during an isentropic process:

$$a^2 = \left. \frac{\partial p}{\partial \rho} \right|_s$$

where the subscript s indicates that the partial derivative is taken holding the entropy, s, fixed. In order to evaluate this expression, we need to determine how pressure and density vary as a function of entropy. In general, the change in entropy is related to the so-called reversible work through the basic thermodynamic relation:

$$T\, ds = de + p\, d(1/\rho)$$

Now for a thermally and calorically perfect gas, we can use this relationship to show that for an isentropic process ($ds = 0$), we have:

$$T p^{-(\gamma-1)/\gamma} = \text{constant}$$

or:

$$p\rho^{-\gamma} = \text{constant}$$

Then, differentiating with respect to ρ yields the expression for the speed of sound given above.

Interestingly, this expression for the speed of sound can be obtained without any direct use of the entropy expression. The approach is to take the one-dimensional fluxes of mass, momentum, and energy to form a flux vector:

$$\mathbf{F} = \begin{pmatrix} \rho u \\ \rho u^2 + p \\ (E+p)u \end{pmatrix}$$

and then compute the Jacobian matrix by differentiating $\mathbf{F}$ with respect to the the conserved flow variables, given by:

$$\mathbf{U} = \begin{pmatrix} \rho \\ \rho u \\ E \end{pmatrix}$$

Then an eigenvalue analysis of the Jacobian matrix gives the characteristic speeds of the flow, which can be related to the propagation of acoustic disturbances. This speed is the acoustic speed, and is given by the equation above. This is physically consistent with the thermodynamic derivation of the sound speed because small pressure (acoustic) disturbances propagate isentropically.

In order to compute the eigenvalues of $A = \frac{\partial \mathbf{F}}{\partial \mathbf{U}}$, we must diagonalize A as

$$A = X^{-1} \Lambda X$$

where X is the matrix of eigenvectors, and Λ is the diagonal matrix of eigenvalues. This can be done by direct computation, but that is tedious. The easier way to do this is to introduce the vector of primitive variables

$$\mathbf{V} = \begin{pmatrix} \rho \\ u \\ p \end{pmatrix}$$

and then to use the chain rule of differentiation for A as:

$$A = \frac{\partial \mathbf{F}}{\partial \mathbf{U}} = \frac{\partial \mathbf{F}}{\partial \mathbf{V}} \frac{\partial \mathbf{V}}{\partial \mathbf{U}} = \frac{\partial \mathbf{U}}{\partial \mathbf{V}} \frac{\partial \mathbf{V}}{\partial \mathbf{U}} \frac{\partial \mathbf{F}}{\partial \mathbf{V}} \frac{\partial \mathbf{V}}{\partial \mathbf{U}} = \left(\frac{\partial \mathbf{V}}{\partial \mathbf{U}} \right)^{-1} \left(\frac{\partial \mathbf{V}}{\partial \mathbf{U}} \frac{\partial \mathbf{F}}{\partial \mathbf{V}} \right) \left(\frac{\partial \mathbf{V}}{\partial \mathbf{U}} \right)$$

Now we can diagonalize $\frac{\partial \mathbf{V}}{\partial \mathbf{U}} \frac{\partial \mathbf{F}}{\partial \mathbf{V}}$ since the outer two matrices are inverses of one another. This is effectively changing variables from $\mathbf{U}$ to $\mathbf{V}$, and then back again.

For a perfect gas, it is easy to compute those matrices, and the result is:

$$\frac{\partial \mathbf{V}}{\partial \mathbf{U}} = \begin{pmatrix} 1 & 0 & 0 \\ -\frac{u}{\rho} & \frac{1}{\rho} & 0 \\ \frac{R}{c_v}\frac{u^2}{2} & -\frac{R}{c_v}u & \frac{R}{c_v} \end{pmatrix}$$

$$\frac{\partial \mathbf{F}}{\partial \mathbf{V}} = \begin{pmatrix} u & \rho & 0 \\ u^2 & 2\rho u & 1 \\ \frac{1}{2}u^3 & \frac{3}{2}\rho u^2 + (1+\frac{c_v}{R})p & (1+\frac{c_v}{R})u \end{pmatrix}$$

This doesn't look too good, but when the two matrices are multiplied together, we get:

$$\frac{\partial \mathbf{V}}{\partial \mathbf{U}}\frac{\partial \mathbf{F}}{\partial \mathbf{V}} = \begin{pmatrix} u & \rho & 0 \\ 0 & u & \frac{1}{\rho} \\ 0 & \gamma p & u \end{pmatrix}$$

Now we find the eigenvalues of this matrix, which is straight-forward. The characteristic equation is

$$(u-\lambda)\big((u-\lambda)^2 - \frac{\gamma p}{\rho}\big) = 0$$

and the eigenvalues are u, $u \pm a$, where a is identified as the speed of sound and is

$$a = \sqrt{\frac{\gamma p}{\rho}} = \sqrt{\gamma R T}$$

which is exactly what was derived previously using the assumption that transmission of sound is an isentropic process.

The isentropic process can be used to derive the total or stagnation variables. These are properties of a flowing gas, and are derived by taking the gas state and adiabatically and isentropically stagnating the gas (bringing it to rest). If the gas is brought to rest through a different process, its state will be different than that given by the stagnation variables. The stagnation temperature has been derived previously, and is proportional to the total (or stagnation) enthalpy:

$$\frac{T_o}{T} = \frac{h_o}{c_p T} = 1 + \tfrac{\gamma-1}{2}M^2$$

Here, T is sometimes called the static temperature, because that would be the temperature measured by a thermocouple traveling at the same speed as the gas – it is static relative to the gas. And T_o is the temperature obtained when the gas is stagnated; its value does not depend on an isentropic process, but only that the process is adiabatic. The stagnation

pressure is computed from the isentropic relation between temperature and pressure given above. Taking the ratio of the stagnation to static conditions yields:

$$\frac{p_o}{p} = \left(\frac{T_o}{T}\right)^{\gamma/(\gamma-1)} = \left(1 + \tfrac{\gamma-1}{2}M^2\right)^{\gamma/(\gamma-1)}$$

This value of pressure is the largest possible pressure that can be obtained from a gas at given static conditions. Any process that is less than ideal (not isentropic) will produce losses and the resulting at-rest pressure will be less than p_o. For this reason, hypersonic inlet efficiency is often expressed in terms of stagnation pressure losses. Such an efficiency would be the ratio of the stagnation pressure of the gas after compression by the inlet to the stagnation pressure of the free-stream gas.

A useful example that uses the concepts discussed so far is the derivation of the Rayleigh Pitot formula. A common means of measuring the state of a supersonic gas is to insert a hollow tube (a Pitot tube) into the flow and measure the stagnation pressure in the tube. Let us derive the pressure measured by the Pitot tube as a function of the upstream conditions. If the static pressure of the gas is known, for example, the Pitot tube will provide a measurement of the Mach number.

The Pitot tube causes the formation of a normal shock wave ahead of the tube; the subsonic flow processed by the shock is then slowly compressed until it stagnates inside the tube. Thus, a fluid element first travels through the normal shock wave (a highly non-isentropic process) and then, because of the slow adiabatic compression, it isentropically comes to rest. Thus, the Pitot tube measures the post-shock stagnation pressure of the gas, $p_{o,2}$. We can compute this value using:

$$p_{o,2} = \frac{p_2}{p_1}\frac{p_{o,2}}{p_2}p_1$$

where the first ratio is the pressure jump across the shock and the second is due to the isentropic compression of the post-shock gas.

Oblique Shock Waves in a Perfect Gas

Now consider how the flow responds to a sudden change in direction (through an angle δ). The figure below shows a supersonic flow traveling parallel to a frictionless plate, and then the flow is turned through a concave corner. An oblique shock wave forms, with angle β relative to the initial flow direction, and the post-shock flow must be parallel to the solid wall. An exact solution exists for this flow, with uniform post shock conditions.

The governing equations are a simple extension of the one-dimensional normal shock equations presented above. First note that the shock-tangent component of the velocity does not change, since there is no variation in flow properties in the tangent direction.

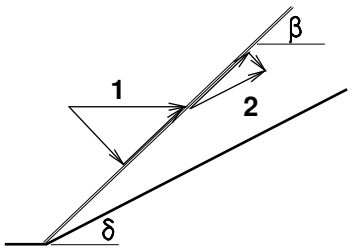

This simplifies the equations to result in:

$$\begin{aligned} \rho_1 u_{n1} &= \rho_2 u_{n2} \\ u_{t1} &= u_{t2} \\ p_1 + \rho_1 u_{n1}^2 &= p_2 + \rho_2 u_{n2}^2 \\ h_1 + \frac{1}{2} u_{n1}^2 &= h_2 + \frac{1}{2} u_{n2}^2 \end{aligned}$$

Some simple analysis shows that the density ratio is related to the shock and turning angles through:

$$\frac{\rho_2}{\rho_1} = \frac{u_{n1}}{u_{n2}} = \frac{\tan\beta}{\tan(\beta - \delta)}$$

The post-shock conditions may be found from the one-dimensional shock relations, by replacing the upstream and downstream Mach numbers with the corresponding shock-normal Mach numbers, $M_{n1} = M_1 \sin\beta$. Thus, for example, the pressure ratio is simply:

$$\frac{p_2}{p_1} = \frac{2\gamma}{\gamma+1} M_{1n}^2 - \frac{\gamma-1}{\gamma+1} = \frac{2\gamma}{\gamma+1} M_1^2 \sin^2\beta - \frac{\gamma-1}{\gamma+1}$$

The oblique shock angle is determined from:

$$\frac{1}{\tan\delta} = \left(\frac{\gamma+1}{2} \frac{M_1^2}{M_1^2 \sin^2\beta - 1} - 1 \right) \tan\beta$$

The results of the oblique shock wave analysis can be plotted in several different ways; the figure below shows how the shock wave angle, β, varies with Mach number for fixed values of the flow turning angle, δ. The limiting case of an infinitesimal disturbance is plotted ($\delta = 0°$), which corresponds to the Mach angle, $\mu = \sin^{-1}(1/M)$.

Note that for a given flow turning angle, there are two possible solutions for β. Under usual conditions, the small shock angle solution is favored. The second solution is termed the strong shock solution, and it is only obtained when the downstream boundary condition

forces a subsonic flow and large pressure rise. Also note that there is a maximum flow turning angle for a given Mach number; if the turning angle is larger than this value, there is no oblique shock solution. In this case, the shock wave is curved and the post-shock flow is not uniform.

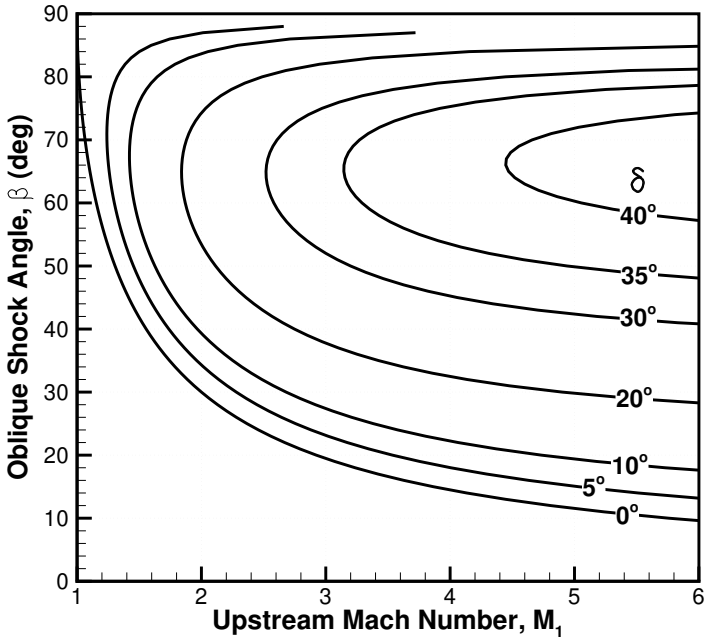

Figure 1. Oblique shock wave angle as a function of upstream Mach number for $\gamma = 1.4$.

Calorically Imperfect Gases

Let us now consider how internal energy is stored in a gas. Air is mostly composed of two diatomic molecules, N_2 and O_2. These molecules store internal energy in three forms: translation, rotation, and vibration. A molecule can have translational (kinetic) energy, and this can be shown to result in an energy per unit mass of:

$$e_{\text{trans}} = \frac{3}{2}\frac{\hat{R}}{M}T$$

where $\hat{R}$ is the universal gas constant and M is the molecular mass of the molecule. In MKS units, $\hat{R} = 8314.3\,\text{J/kmole K}$ and M has units of kg/kmole. Diatomic molecules can be thought of as two masses connected by a spring; the spring represents the interatomic attractive and repulsive force between the two atoms. At low temperature, the spring is not excited and acts like a rigid connection between the atoms. In this case, the energy stored in rotational motion is simply:

$$e_{\text{rot}} = \frac{2}{2}\frac{\hat{R}}{M}T$$

These expressions are best derived from a kinetic theory perspective; such an analysis shows that each degree of freedom of a particle has an energy of $\frac{1}{2}\frac{\hat{R}}{M}T$. Thus, since the particle translates in three dimensions, it has three degrees of freedom; likewise, the diatomic molecule has two non-zero rotational moments of inertia, and therefore two degrees of freedom in rotation. Therefore, a non-linear polyatomic molecule like water would have three rotational degrees of freedom, and its rotational energy would be $\frac{3}{2}\frac{\hat{R}}{M}T$.

The above discussion only applies to internal energy modes that are fully excited – namely the temperature is large enough that all possible quantized energy states are populated. This always applies to translational and rotational energy, except at extremely low temperatures. However, vibrational energy only becomes fully excited at significantly higher temperatures, and we must use a more complicated analysis to derive an expression for the vibrational energy. If we assume that the diatomic molecule acts like a simple harmonic oscillator – that is like two masses connected with an ideal linear spring – we can derive an expression for the energy stored in vibration:

$$e_{\text{vib}} = \frac{2}{2}\frac{\hat{R}}{M}\frac{\theta_v}{e^{\theta_v/T} - 1}$$

where θ_v is the characteristic temperature of vibration for the molecule. Note that in the limit of $T \gg \theta_v$, this expression approaches the expected fully excited energy for

two degrees of freedom. For the vibrational motion, the energy exchanges between the kinetic energy of the atoms and the spring potential energy; thus there are two degrees of freedom. For N_2, $\theta_{v,N_2} = 3395\,\mathrm{K}$ and O_2, $\theta_{v,O_2} = 2239\,\mathrm{K}$ (these values can be measured experimentally).

The above expression for the vibrational energy is approximate because it assumes that the molecule behaves like a simple harmonic oscillator with an infinite number of possible vibrational levels. Also, we have assumed that the vibrational and rotational motion can be treated separately. At high vibrational excitation levels, these assumptions start to break down and it is possible to derive more accurate expressions for the energy stored in the molecule. For our purposes, this expression is sufficiently accurate.

Now, it is a simple matter of adding up the energy stored in each internal mode to obtain the total energy per unit mass of a diatomic molecule:

$$e = e_{\text{trans}} + e_{\text{rot}} + e_{\text{vib}} = \frac{5}{2}\frac{\hat{R}}{M}T + \frac{\hat{R}}{M}\frac{\theta_v}{e^{\theta_v/T} - 1}$$

The specific heat at constant volume can be found be taking the derivative of this expression with respect to T:

$$c_v = \frac{5}{2}\frac{\hat{R}}{M} + \frac{\hat{R}}{M}\left(\frac{\theta_v}{T}\right)^2 \frac{e^{\theta_v/T}}{\left(e^{\theta_v/T} - 1\right)^2}$$

Clearly, the gas is not calorically perfect because the specific heat is not constant. As a result, the ratio of specific heats is also not constant. Therefore, the perfect gas shock relations and stagnation variable relations do not hold; in fact, as we will see, the Mach number is not very useful for high-temperature hypersonic flow applications. Note that when $T \gg \theta_v$, the specific heat approaches $\frac{7}{2}\frac{\hat{R}}{M}$, and $\gamma \to 9/7$.

To get a sense of how important the calorically imperfect effects are, consider a Mach 10 flow of nitrogen; let us compute the stagnation temperature assuming a perfect gas and an imperfect gas. We will assume that the free-stream temperature is 250 K.

Perfect gas:

$$T_o = \left(1 + \tfrac{\gamma-1}{2}M_1^2\right)T_1 = 5250\,\mathrm{K}$$

Imperfect gas:

$$h_o = h_1 + \tfrac{1}{2}u_1^2 = c_p T_1 + \tfrac{1}{2}\left(M_1 a_1\right)^2$$

Since $T_1 = 250\,\mathrm{K}$, we *can* use perfect gas values to compute h_1 and a_1. With $c_p = \frac{7}{2}\frac{\hat{R}}{M}$, $a = \sqrt{\gamma RT}$, and $M = 28.0\,\mathrm{kg/kmole}$, we have $h_o = 5.46 \times 10^6\,\mathrm{J/kg}$. Now we need to solve for T_o, but we only know $h(T)$ and that function is non-linear. Thus, we need to use a

Newton method or some other approach to find T_o. In this case, a Newton method works well and converges to $T_o = 4415\,\mathrm{K}$.

Therefore, the effect of vibrational energy excitation is to absorb additional energy into the internal degrees of freedom, thereby lowering the temperature for a given energy (or enthalpy, in this case). We will see that almost all hypersonic flows of interest involve calorically imperfect gases – in fact, one could argue that this is a necessary property of a hypersonic flow (and certainly a property of a hypervelocity flow).

The above discussion considers how vibrational energy excitation of diatomic gases affects the energy stored in the internal modes. This approach can be extended to molecules with additional vibrational degrees of freedom. For example, consider CO_2, which is a linear triatomic molecule. Therefore, it has two non-zero rotational moments of inertia and its rotational energy storage is the same as a diatomic molecule. However, the vibrational behavior of CO_2 is more complicated due to the additional degrees of freedom that result from having two springs connecting three atoms. A modal analysis shows that the molecule can vibrate in four ways that hold the center of mass of the molecule stationary: the C atom can stay fixed with the two O atoms vibrating symmetrically (symmetric stretch mode); the C atom can move along the axis of the bonds, with the O atoms moving on the same axis (asymmetric stretch); and the two O atoms can move perpendicular to the bond axis, while the C atom moves in the opposite direction (bending mode). The latter motion can take place in two different directions (if bond axis is in the x direction, then the bending can occur in the y and z directions). Thus, there are four independent vibrational modes (with separate characteristic temperatures) and a total of 8 vibrational degrees of freedom. Then, the vibrational energy is obtained by summing the vibrational energy expressions for each mode. Clearly, as the number of atoms increases, the number of vibrational modes increases dramatically.

At very high temperatures, an atom or molecule can become electronically excited. This is an additional means of storing internal energy and must be considered for re-entry at super-orbital speeds. For the time-being, we will not include this process in our analysis.

Here we have only considered calorically imperfect gases. However, gases can also be thermally imperfect, when the thermal equation of state no longer holds. This typically occurs at high pressure when the dilute gas assumption breaks down, and when the gas is so dense that the volume taken up by the particles cannot be neglected.

Shock Waves in Imperfect Gases

Now let us consider a shock wave in a calorically imperfect gas; for this example, we will assume that it is a single diatomic species so that the above equations of state hold. The one-dimensional mass, momentum, and energy conservation equations hold, but it is no longer possible to obtain a closed-form solution in terms of the Mach number and ratio of specific heats. As we saw above, γ is not a constant, and therefore it is not useful to use in the analysis. Rather, we must solve the equations directly.

If we substitute the density ratio across the shock into the momentum and energy equations, we obtain:

$$p_2 = p_1 + \rho_1 u_1^2 \left(1 - \frac{\rho_1}{\rho_2}\right)$$

$$h_2 = h_1 + \tfrac{1}{2} u_1^2 \left(1 - \frac{\rho_1^2}{\rho_2^2}\right)$$

In addition, we have $p = \rho RT$ and $h = h(T)$. An iterative solution approach is as follows:

1. guess ρ_2
2. compute p_2 and h_2
3. use a Newton method to solve for T_2 using $h(T_2) = h_2$
4. obtain new guess for $\rho_2' = p_2/RT_2$
5. is $\rho_2' = \rho_2$? If yes, done; if not go to 1.

If we take the Mach 10 conditions given above and assume that the free-stream density is $\rho_1 = 0.01\,\mathrm{kg/m^3}$, let us compute the post-shock conditions.

At these conditions, $u_1 = 3224\,\mathrm{m/s}$, $p_1 = 742.3\,\mathrm{Pa}$.

Assume $\rho_2 = 6\rho_1$ (from perfect gas relations with $M_1 \to \infty$).

Iteration 1: $p_2 = 87360\,\mathrm{Pa}, h_2 = 5.313\,\mathrm{MJ/kg} \Rightarrow \mathrm{T}_2 = 4304\,\mathrm{K}$. Then $\rho_2' = \frac{p_2}{RT_2} = 0.06835\,\mathrm{kg/m^3}$. Use this value of density for iteration 2.

Iteration 2: $p_2 = 89480\,\mathrm{Pa}, h_2 = 5.346\,\mathrm{MJ/kg} \Rightarrow \mathrm{T}_2 = 4329\,\mathrm{K}$. Then $\rho_2' = \frac{p_2}{RT_2} = 0.06960\,\mathrm{kg/m^3}$.

We want the assumed density equal to the computed density: $\rho_a = \rho_c$; we can then solve for the point where the two lines intersect. Taking the values above, we can show:

$$\frac{\rho_c}{\rho_1} = 0.1497 \frac{\rho_a}{\rho_1} + 5.9368$$

Then, with $\rho_c = \rho_a$, we have a new guess for $\rho_2/\rho_1 = 6.982$.

Iteration 3: $p_2 = 89800\,\text{Pa}, h_2 = 5.350\,\text{MJ/kg} \Rightarrow \text{T}_2 = 4332\,\text{K}$. Then $\rho_2' = \frac{p_2}{RT_2} = 0.06981\,\text{kg/m}^3$.

Therefore, the post-shock conditions are:

$$\rho_2/\rho_1 = 6.98, T_2/T_1 = 17.3, p_2/p_1 = 121$$

Compare these results to perfect gas:

$$\rho_2/\rho_1 = 5.71, T_2/T_1 = 20.4, p_2/p_1 = 117$$

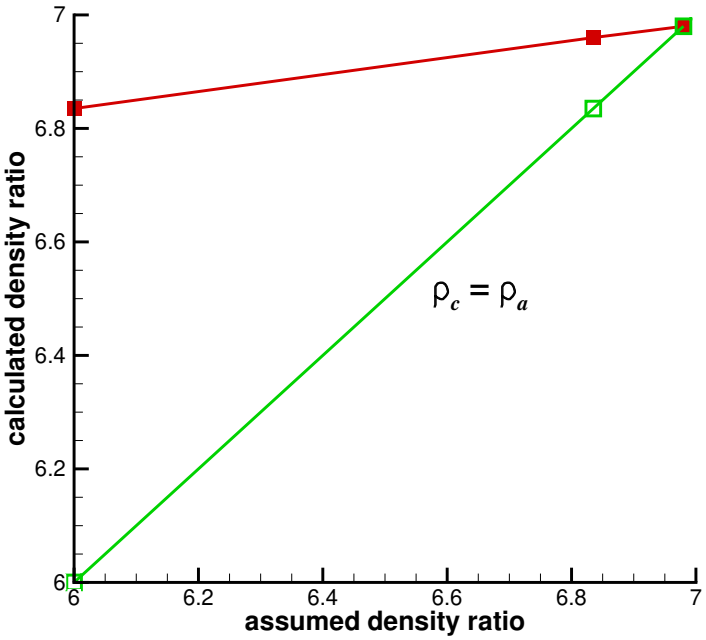

Figure 2. Computed density ratio versus guessed density ratio.

The above result is general in the sense that imperfect gas effects have little effect on the post-shock pressure, increase the density ratio, and decrease the temperature ratio.

Shock Waves with Chemically Reacting Gas

In the previous analysis, we had a constant value for the gas constant, $R = \frac{\hat{R}}{M}$. However, at relevant post-shock temperatures, the gas will react and the molecular weight will change. Therefore, we must modify the analysis to include this effect.

For example, air can react to form several chemical species:

$$\mathrm{N_2} \leftrightarrow 2\mathrm{N}$$

$$\mathrm{O_2} \leftrightarrow 2\mathrm{O}$$

$$\mathrm{NO} \leftrightarrow \mathrm{N} + \mathrm{O}$$

$$\mathrm{N_2} + \mathrm{O} \leftrightarrow \mathrm{NO} + \mathrm{N}$$

$$\mathrm{O_2} + \mathrm{N} \leftrightarrow \mathrm{NO} + \mathrm{O}$$

These reactions start to occur at appreciable levels at about 2000 K.

The mixture gas constant is computed by mass weighting the individual gas constants. This can be obtained by noting that the pressure is the sum of the partial pressures:

$$p = \sum_s p_s = \sum_s \frac{\rho_s \hat{R} T}{M_s} = \rho R T$$

Here ρ_s is the density of species s, and the summations are over all possible chemical species. Then we have:

$$R = \hat{R} \sum_s \frac{\rho_s}{\rho M_s} = \hat{R} \sum_s \frac{c_s}{M_s}$$

where $c_s = \rho_s / \rho$ is the mass fraction of species s.

Each of the above reactions has a temperature-dependent equilibrium constant; for example, for the nitrogen dissociation reaction, we have:

$$K_{eq}(T) = \frac{[\mathrm{N}]^2}{[\mathrm{N_2}]}$$

where the square brackets denote the molar concentration of the particular species. For example, $[\mathrm{N}] = \rho_\mathrm{N} / M_\mathrm{N}$. The equilibrium constants can be computed by minimizing the Gibbs free energy for each reaction; typically they are then curve-fitted for a range of temperatures. Given a value for each equilibrium constant, it is then possible to compute the equilibrium mixture of the gas at a given pressure and temperature.

For example, let us consider the case of nitrogen at high temperature, so that it is dissociated. From the expressions for the equilibrium constant and pressure, we have

$$\left(\frac{\rho_\mathrm{N}}{M_\mathrm{N}} \right)^2 = K_{eq} \frac{\rho_{\mathrm{N_2}}}{M_{\mathrm{N_2}}}$$

$$p = \frac{\rho_\mathrm{N} \hat{R} T}{M_\mathrm{N}} + \frac{\rho_{\mathrm{N_2}} \hat{R} T}{M_{\mathrm{N_2}}}$$

Therefore, we can solve for the species densities, given a pressure and temperature; we can then compute all other mixture properties such as enthalpy. In the case of air, we use equilibrium constant expressions for the first three reactions shown above (the additional reactions do not add information and are redundant). We use the fact that the ratio of oxygen atoms to nitrogen atoms in the mixture cannot change, and that gives sufficient information to solve for the mixture composition at a given pressure and temperature.

We will not go into the details of how the equilibrium composition is computed, but will focus on using the results of that computation. The figures below plot temperature as a function of enthalpy and pressure, and Z, which is called the compressibility and is defined such that:

$$p = \rho \bar{R} T Z$$

where $\bar{R} = \hat{R}/28.96$ is the gas constant for unreacted air. Thus, $Z = R/\bar{R}$ and is a measure of how much the gas constant has changed due to chemical reactions.

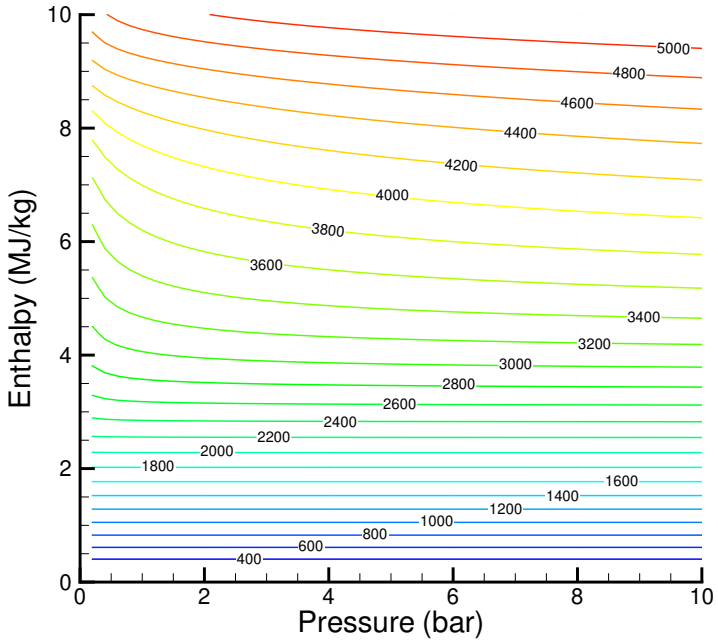

Figure 3. Variation of temperature with pressure and enthalpy for air.

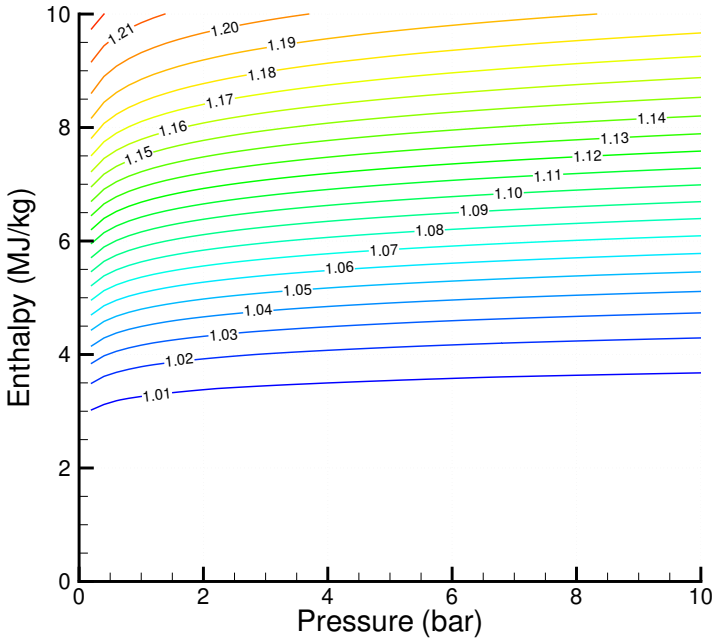

Figure 4. Variation of compressibility, Z, with pressure and enthalpy for air.

Now let us return to the computation of post-shock conditions for the reacting gas. For simplicity, define $\epsilon = \rho_1/\rho_2$, which is the ratio of the free-stream density to the post-shock density. Then the basic shock relations are:

$$p_2 = p_1 + \rho_1 u_1^2 (1 - \epsilon)$$
$$h_2 = h_1 + \tfrac{1}{2} u_1^2 (1 - \epsilon^2)$$

The solution approach is exactly the same as discussed above, but there is an additional step involving the compressibility:

1. guess ϵ
2. compute p_2 and h_2
3. compute T_2 and Z_2 from equilibrium gas solver
4. compute $\epsilon' = \frac{\rho_1}{\rho_2'} = \rho_1 \frac{\bar{R} T_2 Z_2}{p_2} = \frac{p_1}{p_2} \frac{T_2}{T_1} Z_2$
5. is $\epsilon' = \epsilon$? If yes, done; if not go to 1.

Consider the previous problem, but use air instead of nitrogen for the gas. With the change in gas constant, the free-stream speed and pressure are 3170 m/s and 717.7 Pa. We'll use the previous result as the guess for $\epsilon = 1/6.98$.

Iteration 1: $p_2 = 86810\,\mathrm{Pa}, h_2 = 5.173\,\mathrm{MJ/kg} \Rightarrow \mathrm{T}_2 = 3326\,\mathrm{K}, \mathrm{Z}_2 = 1.0605$. Then $\epsilon' = \frac{p_1}{p_2}\frac{T_2}{T_1}Z_2 = 0.1167\,\mathrm{kg/m^3}$.
Following a similar approach as in the previous example, we find a converged value of $\epsilon = 0.113 = 1/8.82$; $T_2 = 3339\,\mathrm{K}$ and $p_2 = 89820\,\mathrm{Pa}$.

The above computations were performed with a Matlab code that will be distributed. Another approach is to use the NASA CEA (Chemical Equilibrium with Applications) code; this is available from NASA as a Fortran code or it can be run with a web-based tool (`http://cearun.grc.nasa.gov/index.html`). The web-based tool is a simple front-end to the old-fashioned Fortran code.

One of the applications within CEA is the normal shock problem that we have just discussed, and it can be used to solve many of the problems in the course. The results obtained above are consistent with those from CEA; note that CEA uses a reference temperature of 298.15 K rather than zero, which is what we will use throughout the course. For the Mach 10 condition discussed above, CEA shows that the post-shock flow has about equal mole fractions of oxygen molecules and oxygen atoms. Thus about 1/3 of the oxygen is dissociated at this condition.

Stagnation Point Flow

Now consider what happens when the gas passes through a shock wave and then stagnates on the nose of a hypersonic vehicle. Figure 5 shows a CFD simulation of 4000 m/s air flowing over a sphere (this is an inviscid simulation with free-stream conditions corresponding to an altitude of 40 km). The variable plotted is the pressure to free-stream pressure ratio. Note that there is a huge jump in pressure across the shock (usually called the bow-shock) and then a weak compression to the stagnation point; for this case, the computed pressure ratio at the stagnation point is 210.7.

To compute the conditions at the stagnation point, we have to integrate the pressure change from the post-shock state to the stagnated state. In the low speed post-shock flow, we will assume that the density is nearly constant, and then we can integrate exactly the Euler equation (which is a differential form of the momentum equation):

$$
\begin{aligned}
dp &= -\rho u\, du \\
\int_p^{p_o} dp &= -\rho \int_u^0 u\, du \\
p_o - p &= \tfrac{1}{2}\rho u^2
\end{aligned}
$$

Combining this result with the shock relations gives:

$$\begin{aligned} p_o &= p_2 + \tfrac{1}{2}\rho_2 u_2^2 \\ p_o &= p_1 + \rho_1 u_1^2\Big(1 - \frac{\epsilon}{2}\Big) \\ h_o &= h_1 + \tfrac{1}{2}u_1^2 \end{aligned}$$

The pressure coefficient at the stagnation point may be computed as:

$$C_{po} = \frac{p_o - p_1}{\frac{1}{2}\rho_1 u_1^2} = 2 - \epsilon$$

Note that there is a weak dependence on the density ratio, and that as the density ratio increases, the pressure coefficient approaches 2.

The solution to the stagnation point problem proceeds in a similar fashion to the post-shock computation. However, it is slightly more straight-forward because the stagnation enthalpy is constant.

If we return to our Mach 10 air example, we can compute the post-shock conditions with CEA, for example. Then use the Bernoulli equation to stagnate the post shock gas. For the conditions of $\rho_1 = 0.01\,\mathrm{kg/m^3}$ and $T_1 = 250\,\mathrm{K}$, CEA gives very similar results to the previous example (computed with mollier.m): $p_2 = 89890\,\mathrm{Pa}$, $u_2 = 358.6\,\mathrm{m/s}$, $T_2 = 3337.2\,\mathrm{K}$, and $s_2 = 10.084\,\mathrm{kJ/kg\,K}$.

With $p_o = p_2 + \frac{1}{2}\rho_2 u_2^2$ and $h_o = h_1 + \frac{1}{2}u_1^2$, we find $p_o = 95310\,\mathrm{Pa}$ and $h_o = 4.974\,\mathrm{MJ/kg}$. This gives a pressure coefficient of $C_{po} = 1.883$ and a density ratio of $\rho_o/\rho_1 = 8.52$. The latter is clearly wrong since the shock calculation produces a density of $\rho_2/\rho_1 = 8.82$. This result shows that stagnation point computation is approximate (though still fairly accurate).

We can obtain the exact stagnation point conditions using CEA in an iterative fashion. We know that the process going from state 2 to stagnation is adiabatic and isentropic. Therefore, the stagnation state produces the same total enthalpy and entropy as the post-shock state obtained from CEA. This requires some iterations in pressure and temperature to solve for the actual stagnation condition. (Unfortunately, the constant *sp* process is not functional in the online version of CEA.) With some trial and error and bracketing of the results, the exact stagnation conditions are found to be: $p_o = 95700\,\mathrm{Pa}$, $T_o = 3361.2\,\mathrm{K}$, and $\rho_o = 0.09332$. This produces $C_{po} = 1.890$, which is very close to the approximate value (within 0.4%).

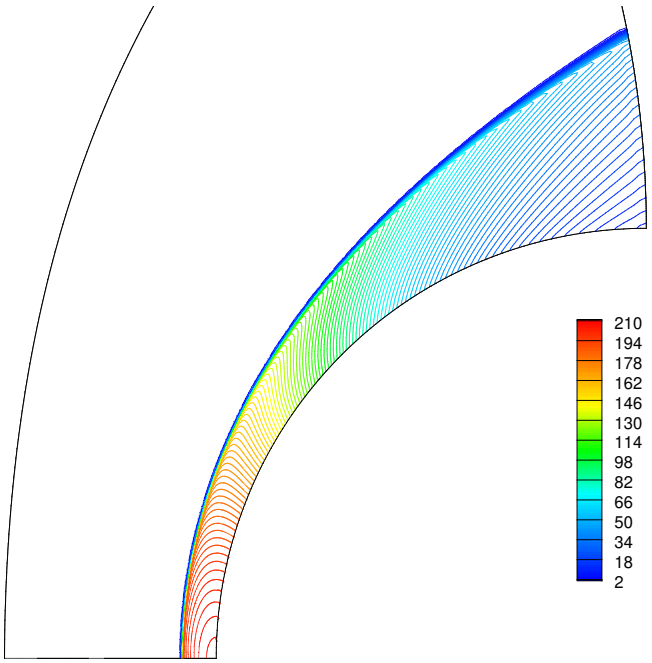

Figure 5. Non-dimensional pressure from a CFD calculation of the inviscid flow of air over a sphere at 40 km altitude.

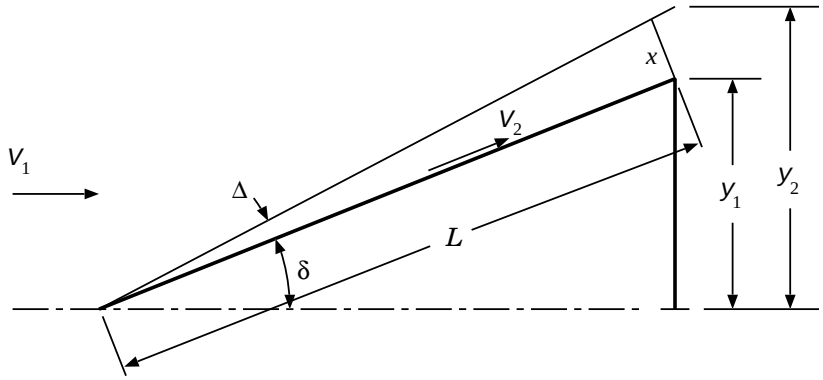

Figure 6. Schematic of wedge flow for computation of post-shock conditions.

Oblique Shock Waves in Chemically Reacting Gases

There is of course no exact solution for an oblique shock wave in a reacting mixture of gases. However, we can derive an approximate result using some geometry and the iterative solution of modified shock wave equations. Consider the schematic of flow over a two-dimensional wedge in Figure 6. We denote the magnitude of the velocity as V, and the shock angle relative to the wedge as Δ. Then from continuity, we have:

$$\rho_1 V_1 y_2 = \rho_2 V_2 x$$

and defining ϵ as the inverse density ratio, we have:

$$\epsilon = \frac{\rho_1}{\rho_2} = \frac{V_2}{V_1}\frac{y_1}{y_2}\frac{x}{y_1}$$

Now using a small angle approximation, we can write the relative shock angle in terms of the ϵ:

$$\Delta \simeq \tan\Delta = \frac{x}{L} = \frac{x\sin\delta}{y_1}$$

and

$$\Delta = \frac{\epsilon\tan\delta}{1-\epsilon}$$

The shock relations are modified through the use of the shock-normal velocity, as with the perfect gas oblique shock relations.

$$p_2 = p_1 + \rho_1 V_1^2\big(1-\epsilon\big)\sin^2\beta$$
$$h_2 = h_1 + \tfrac{1}{2}V_1^2\big(1-\epsilon^2\big)\sin^2\beta$$

The shock angle, β, is equal to $\delta + \Delta$. Finally, we obtain the pressure coefficient as:

$$C_{pw} = \frac{2\sin^2\delta_w}{1-\epsilon}$$

where the subscript w indicates that the expression holds for a wedge. Obviously, the above expressions must be solved in an iterative fashion, very similar to the normal shock relations.

For an example, consider the Mach 20 flow over a 20 degree wedge flying at 32 km altitude. Here the free-stream conditions are $T_1 = 226.15\,\mathrm{K}$, $p_1 = 900\,\mathrm{K}$, $\rho_1 = 0.01388\,\mathrm{kg/m^3}$, and $V_1 = 6017\,\mathrm{m/s}$. Table 1 compares the approximate oblique shock theory to perfect gas oblique shock theory and to a CFD solution obtained with an equilibrium equation of state.

The primary approximation made above is the small angle approximation for $\tan\Delta$. For high Mach number flows, the relative shock angle is usually small and this approximation is quite accurate. This accounts for the remarkably good comparison between equilibrium gas theory and CFD. Also, note that the expression for the wedge pressure coefficient is proportional to $\sin^2\delta_w$ and has only a weak dependence on the density ratio across the shock.

Table 1 Comparison of theory and CFD for Mach 20 wedge flow.

	Perf. Gas	Eq. Theory	Eq. CFD
Δ(deg)	4.70	3.54	3.67
ρ_2/ρ_1	5.60	6.891	6.885
T_2/T_1	14.51	11.15	11.19
p_2/p_1	81.29	77.14	77.42

Cone Flow in Chemically Reacting Gases

The flow over a cone does not have a closed form exact solution for a perfect gas because the post-shock flow is non-uniform. The flow is self-similar and an ordinary differential equation in a single variable can be derived to describe the flow. This is Taylor-Maccoll theory. For the reacting gas case, we have to make further approximations to obtain reasonable estimates of the conical pressure distribution. One such approach is to assume that about half of the normal-direction post-shock momentum is transferred to the surface. Then the cone pressure is approximated by:

$$p_c \simeq p_2 + \rho_2\left(\tfrac{1}{2}u_2\right)^2$$

where u_2 is the surface-normal component of the post-shock pressure.

Thus, the approach is to use the oblique shock flow discussed above; compute the post-shock pressure as before, but reduce the shock angle to account for reduced momentum transfer to the surface. Then we have the approximate relations:

$$\Delta_c = \frac{\epsilon\tan\delta_c}{2-\epsilon}, \sin\beta = \frac{\sin\delta_c}{1-\epsilon/2}$$

Then the cone pressure coefficient is given by:

$$C_{pc} = \frac{2\sin^2\delta_c}{1-\epsilon/4}$$

Again, note that the pressure coefficient scales with $\sin^2\delta_c$ and the dependence on the density ratio is weaker than for a wedge.

Mach Number Independence

Certain flow parameters are weak functions of the free-stream Mach number in the limit of large Mach number. We have seen this in the equilibrium gas pressure coefficients which depend on ϵ, which is a weak function of free-stream Mach number. We can also show this independence using the perfect gas shock relations and taking the limit as M_1 approaches infinity.

We previously showed that the limiting density ratio is

$$\frac{\rho_2}{\rho_1} \to \frac{\gamma+1}{\gamma-1}$$

as $M_1 \to \infty$.

For an oblique shock, we have:

$$\frac{p_2}{p_1} = 1 + \frac{2\gamma}{\gamma+1}\left(M_1^2 \sin^2\beta - 1\right)$$
$$C_p = \frac{p_2 - p_1}{\frac{1}{2}\rho_1 u_1^2} = \frac{2}{\gamma M_1^2}\left(\frac{p_2}{p_1} - 1\right)$$

in the limit of $M_1 \to \infty$, we have:

$$\frac{p_2}{p_1} \to \frac{2\gamma}{\gamma+1} M_1^2 \sin^2\beta$$
$$C_p \to \frac{4}{\gamma+1}\sin^2\beta$$

Thus, within the limits of this analysis, the pressure coefficient is independent of Mach number.

The oblique shock angle is given by:

$$\tan\delta = 2\cot\beta\left[\frac{M_1^2\sin^2\beta - 1}{M_1^2(\gamma + \cos 2\beta) + 2}\right]$$

for $M_1 \to \infty$,

$$\beta \to \frac{\gamma+1}{2}\delta$$

which is also independent of M_1. The previous wedge calculation for $M_1 = 20$, gave a shock angle of $\beta = 24.7°$. The above expression gives $\beta = 24°$ for $\gamma = 1.4$.

Newtonian Aerodynamics

In the *Principia*, Sir Isaac Newton proposed a model for the drag acting on a boat, in which the incoming stream loses all of its normal-direction momentum to the surface of

the boat, and the tangential component of momentum is conserved. This is a very poor representation of the flow of water over a slowly-moving boat, but under some conditions it is a reasonable model of the flow over hypersonic vehicles.

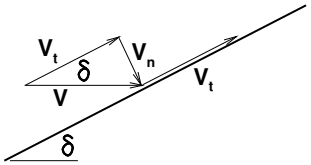

The Newtonian aerodynamics pressure coefficient can be derived by recognizing that the surface pressure is equal to the change in normal momentum times the flux of mass normal to the surface:

$$p_2 - p_1 = V_1 \sin\delta \times \rho_1 V_1 \sin\delta = \rho_1 V_1^2 \sin^2\delta$$

and then

$$C_p = 2\sin^2\delta$$

In general, if we define the surface-normal unit vector to be $\hat{n}$ and the free-stream velocity as $\vec{V}_1 = V_1\hat{v}_1$ then the surface-normal momentum conservation is:

$$p_1 + \rho_1\big(\vec{V}_1 \cdot \hat{n}\big)^2 = p_2 + \rho_2\big(\vec{V}_2 \cdot \hat{n}\big)^2$$

But for Newtonian aerodynamics, $\vec{V}_2 \cdot \hat{n} = 0$ and then we obtain:

$$C_p = 2\big(\hat{v}_1 \cdot \hat{n}\big)^2$$

Thus, the local surface pressure depends only on the orientation of the surface relative to the free-stream. For those parts of the geometry that are not impacted by the incoming stream, we usually assume that the pressure coefficient is zero ($p_2 = p_1$). This makes it simple to integrate over a vehicle to determine its lift and drag coefficients.

For example, we can compute the lift and drag coefficients of a wedge as shown in the figure below. Here the pressure on the forward-facing part of the wedge has a value of:

$$p_2 = p_1 + \rho_1 V_1^2 \sin^2\delta$$

and the pressure on the other two faces is taken to be p_1 because there is no component of free-stream velocity impacting those surfaces.

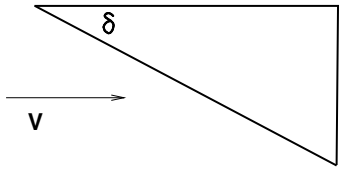

If we let the length of wedge face be ℓ, then the lift and drag forces (per unit depth into the page) acting on the body are:

$$D = p_2 \ell \sin\delta - p_1 \ell \sin\delta$$
$$L = p_2 \ell \cos\delta - p_1 \ell \cos\delta$$

Now, by convention we take the reference area to be equal to the wedge base area: $A_{\text{ref}} = \ell \sin\delta$. Then we obtain the lift and drag coefficients as:

$$C_D = 2\sin^2\delta$$
$$C_L = 2\sin\delta\cos\delta$$

and the lift-to-drag ratio is $L/D = \cot\delta$.

We can also compute the drag coefficient for a cone flying at zero angle of attack, as shown in the figure below. Here, we have to integrate over the surface to compute the drag. If x is in the direction of the velocity vector, we need to solve the integral:

$$D = \int\int p_2(-n_x)\, dA$$

and then use the base area as the reference area to compute the drag coefficient.

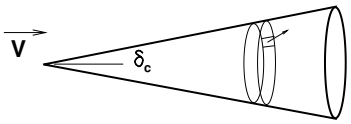

Performing this integration is straight-forward, but a little tricky. Instead, let us consider what the cone looks from a front view. Clearly, the flow is turned through an angle of δ_c, resulting in a surface pressure of $p_2 = p_1 + \rho_1 V_1^2 \sin^2\delta_c$. The projection of this pressure into the x direction results in p_2 acting over an area equal to the cone base area. Therefore, the drag can easily be computed as:

$$D = p_2 A_{\text{ref}} - p_{\text{base}} A_{\text{base}} = (p_2 - p_1) A_{\text{ref}}$$

Therefore, the drag coefficient is simply:

$$C_D = 2\sin^2\delta_c$$

which is as expected.

Modified Newtonian Aerodynamics

Newtonian aerodynamics predicts that the stagnation point pressure coefficient is $C_{po} = 2$, but we have seen from the equilibrium gas analysis that $C_{po} = 2 - \epsilon$. For a perfect gas analysis, we can take the limit of infinite free-stream Mach number in the Rayleigh Pitot pressure formula to show:

$$C_{po} \to \Big(\frac{4}{\gamma+1}\Big)\Big(\frac{(\gamma+1)^2}{4\gamma}\Big)^{\gamma/\gamma-1}$$

Which for $\gamma = 1.4$ gives $C_{po} = 1.839$. Clearly, Newtonian aerodynamics over-predicts the stagnation point pressure.

Lester Lees (1955) recognized this problem and proposed a modification to Newtonian aerodynamics. The idea is to compute the stagnation point value of the pressure coefficient, and then compute the local pressure from:

$$C_p = C_{po}\sin^2\delta$$

Thus, modified Newtonian aerodynamics predicts lower surface pressures by the ratio of $C_{po}/2$.

It is interesting to compare Newtonian and modified Newtonian aerodynamics with computational fluid dynamics. For example, Figure 7 plots the pressure coefficient on the Mars Science Lab (MSL) heat shield (sphere-70° cone) at zero angle of attack. Newtonian aerodynamics over-predicts the stagnation point pressure, and under-predicts the pressure on the cone; the Lees modification makes the stagnation point pressure agree, but makes the under-prediction on the cone worse. Note that neither approach correctly represents the over-expansion and recompression that occur at the sphere-cone junction.

These discrepancies are typical of how well Newtonian aerodynamics performs; clearly it is not exact, but it is representative of the pressure distribution. Also, the errors at the stagnation point sometimes offset the overall differences, making un-modified Newtonian aerodynamics fortuitously more accurate for aerodynamic coefficients.

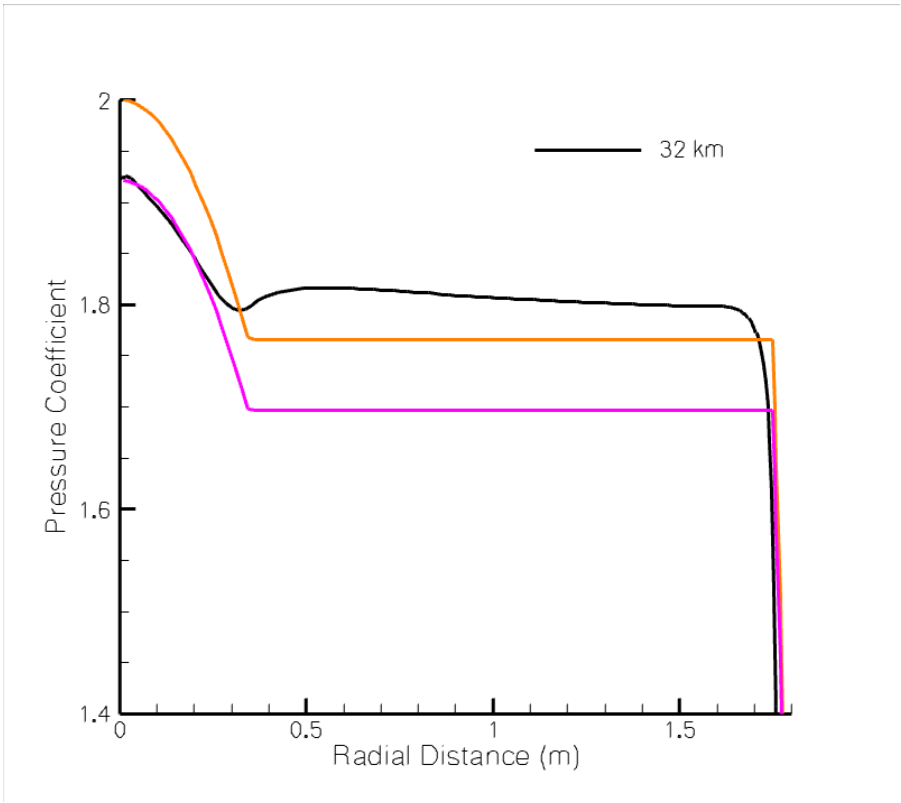

Figure 7. Surface pressure coefficient on the MSL geometry at zero angle of attack: CFD (black); Newtonian aerodynamics (orange); modified Newtonian aerodynamics (pink).

Hypersonic Similarity Parameter

Consider the perfect gas oblique shock relation between the flow turning angle, δ, and the shock angle, β.

$$\tan\delta = 2\cot\beta\left[\frac{M_1^2\sin^2\beta - 1}{M_1^2(\gamma + \cos 2\beta) + 2}\right]$$

For small angles and large M_1, we can obtain a quadratic function of β/δ, which has one meaningful root:

$$\frac{\beta}{\delta} = \frac{\gamma+1}{4} + \sqrt{\left(\frac{\gamma+1}{4}\right)^2 + \frac{1}{M_1^2\delta^2}}$$

This is a different result than we obtained in the hypersonic limit ($\beta/\delta = (\gamma+1)/2$) because we have taken small angle limits; note if the second term in the square root is small, then we obtain the previous result.

Now, for small shock angles the pressure ratio is

$$\frac{p_2}{p_1} = 1 + \frac{2\gamma}{\gamma+1}\left(M_1^2\beta^2 - 1\right)$$

and substituting the previous result for β gives

$$\frac{p_2}{p_1} = 1 + \frac{\gamma(\gamma+1)}{4} M_1^2 \delta^2 + \gamma \sqrt{\left(\frac{\gamma+1}{4}\right)^2 + \frac{1}{M_1^2 \delta^2}} M_1^2 \delta^2$$

Define the hypersonic similarity parameter as: $K = M_1 \delta$. Then we have:

$$\frac{p_2}{p_1} = 1 + \frac{\gamma(\gamma+1)}{4} K^2 + \gamma K^2 \sqrt{\left(\frac{\gamma+1}{4}\right)^2 + \frac{1}{K^2}}$$

and the pressure coefficient is

$$C_p = 2\delta^2 \Big[\frac{\gamma+1}{4} + \sqrt{\left(\frac{\gamma+1}{4}\right)^2 + \frac{1}{K^2}} \Big] = C_p(\delta, K)$$

Note that the pressure ratio only depends on the hypersonic similarity parameter, and that the pressure coefficient has the expected quadratic variation with flow turning angle. As seen previously, Newtonian aerodynamics tends to under-predict wedge pressures; for small-angle cones, this result is generally more accurate.

A similar derivation may be performed for the hypersonic expansion flow (here the flow turns away from itself through an angle θ). The Prandtl-Meyer result is usually written as:

$$\theta = \nu(M_2) - \nu(M_1)$$

where ν is the Prandtl-Meyer function

$$\nu(M) = \sqrt{\frac{\gamma+1}{\gamma-1}} \Big[\tan^{-1} \sqrt{\frac{\gamma-1}{\gamma+1}(M^2-1)} \Big] - \tan^{-1} \sqrt{M^2-1}$$

We can write $\tan^{-1}$ as a series expansion

$$\tan^{-1} \frac{1}{M} = \frac{1}{M} - \frac{1}{3M^3} + \frac{1}{5M^5} - \cdots$$

Also note that $\tan^{-1} M = \frac{\pi}{2} - \tan^{-1} \frac{1}{M}$. Then in the limit of $M \gg 1$, we have

$$\theta = \frac{2}{\gamma-1} \Big(\frac{1}{M_1} - \frac{1}{M_2} \Big)$$

Or

$$\frac{M_2}{M_1} = \frac{1}{1 - \frac{\gamma-1}{2} K}$$

The flow through the expansion is isentropic, and therefore we obtain

$$\frac{p_2}{p_1} \simeq \Big(\frac{M_1^2}{M_2^2} \Big)^{\gamma/\gamma-1} = \Big(1 - \tfrac{\gamma-1}{2} K \Big)^{2\gamma/\gamma-1}$$

and the pressure coefficient is

$$C_p = \frac{2\theta^2}{\gamma K^2}\left[\left(1 - \tfrac{\gamma-1}{2}K\right)^{2\gamma/\gamma-1} - 1\right]$$

Again, note that the pressure ratio across the expansion depends only on K, while the pressure coefficient is proportional to the turning angle squared.

Effective γ Calculations

The classic hypersonic flow literature often uses the concept of an "effective γ" to mimic the effects of internal energy relaxation and chemical reactions. The idea is to use a value of γ in the perfect gas shock relations so as to recover the correct reacting gas conditions. For example, a typical approach would be to represent the post-shock pressure coefficient as:

$$C_{p2} = \frac{2}{\gamma_1 M_1^2}\left(\frac{p_2}{p_1}\Big|_{\gamma_2} - 1\right)$$

where the pressure ratio is evaluated using a post-shock value of $\gamma = \gamma_2$. We will see that this approach is not valid.

The pressure ratio is derived starting from the definition of enthalpy at the post-shock state:

$$h_2 = c_p T_2 = \frac{\gamma_2}{\gamma_2 - 1} R_2 T_2 = \frac{\gamma_2}{\gamma_2 - 1}\frac{p_2}{\rho_2}$$

where γ_2 is chosen so that for a given T_2, we have

$$h_2 = \int_0^{T_2} c_p \, dT = \frac{\gamma_2}{\gamma_2 - 1} R_2 T_2$$

Now from the momentum conservation equation, we have

$$V_1^2 = \left(\frac{\rho_2}{\rho_1}\right)\left(\frac{p_2 - p_1}{\rho_2 - \rho_1}\right)$$
$$V_2^2 = \left(\frac{\rho_1}{\rho_2}\right)\left(\frac{p_2 - p_1}{\rho_2 - \rho_1}\right)$$

Now from total enthalpy conservation, we have:

$$h_2 - h_1 = \frac{\gamma_2}{\gamma_2 - 1}\frac{p_2}{\rho_2} - \frac{\gamma_1}{\gamma_1 - 1}\frac{p_1}{\rho_1} = \frac{1}{2}\left(\frac{1}{\rho_1} + \frac{1}{\rho_2}\right)(p_2 - p_1)$$

Then we can solve for the pressure ratio as

$$\frac{p_2}{p_1} = \left(\frac{\gamma_2 - 1}{\gamma_1 - 1}\right)\frac{\frac{\rho_2}{\rho_1}(\gamma_1 + 1) - (\gamma_1 - 1)}{(\gamma_2 + 1) - \frac{\rho_2}{\rho_1}(\gamma_2 - 1)}$$

The density ratio is obtained from the V_1 expression and the free-stream Mach number. This results in a quadratic that can be solved for $\frac{\rho_2}{\rho_1}$ in terms of the two values of γ.

$$\left(\frac{\rho_2}{\rho_1}\right)^2\left[\gamma_1 M_1^2(\gamma_2-1)+2\gamma_1\frac{\gamma_2}{\gamma_1-1}\right]-\left(\frac{\rho_2}{\rho_1}\right)\left[2\gamma_1\gamma_2 M_1^2\right]+\gamma_1 M_1^2(\gamma_2+1)=0$$

Thus, in principle, it is possible to find the γ_2 that satisfies these relationships. However, to do so correctly involves finding R_2 and T_2 from h_2; which is essentially equivalent to the previous iterative approach.

In practice, the effective γ approach is typically used with an assumed value of γ_2. Then the above relations are closed, and it is possible to solve for the pressure coefficient directly. This is of course approximate and is often justified by the observation that γ_2 is a slowly varying function of the free-stream flow conditions. However, this is obviously the case since γ has limits over a narrow range of values and approaches unity for infinitely strong shock waves.

The worst thing about the effective γ approach is that it confuses the underlying gas dynamics and tries to make a perfect gas representation somehow work for an imperfect gas. Remember that γ is used in two ways during the derivation of the perfect gas shock relations: (1) to relate the specific heat to the gas constant ($c_p/R = \gamma/(\gamma-1)$) in the enthalpy equation; and (2) to relate the kinetic energy to the internal energy through the speed of sound.

II. Viscous Hypersonic Flows

Most hypersonic flows occur at high altitude where the density is low, and as a result, the Reynolds number is relatively low. Thus, viscous effects are more important than in conventional aerodynamics flows. In addition, a critical design parameter is the level of aerodynamic heating of the vehicle, and this is a viscous flow effect. We focus on two exact solutions of the boundary layer equations for perfect gases: compressible flow on a flat plate or wedge, and stagnation point flow. We then extend the stagnation point solution to account for chemical reactions and chemical recombination at the surface of a vehicle. Finally, we consider several advanced topics including viscous-inviscid interactions and shock wave / boundary layer interactions.

Boundary Layer Analysis

Consider the flow over a two-dimensional or axisymmetric hypersonic vehicle; we assume that the boundary layer is thin relative to the characteristic length, L, of the vehicle. That is, if δ is the boundary layer thickness, then $\delta \ll L$. We adopt a coordinate system with x running along the body, and y running perpendicular to the surface at all x. As with incompressible boundary layer flow, we non-dimensionalize the equations and neglect terms of order δ/L.

The resulting compressible boundary layer equations for a single-species gas are:

$$\begin{aligned}
\frac{\partial}{\partial x}(\rho u) + \frac{\partial}{\partial y}(\rho v) &= 0 \\
\rho u \frac{\partial u}{\partial x} + \rho v \frac{\partial u}{\partial y} &= -\frac{\partial p_e}{\partial x} + \frac{\partial}{\partial y}\Big(\mu \frac{\partial u}{\partial y}\Big) \\
\frac{\partial p}{\partial y} &= 0 \\
\rho u \frac{\partial h}{\partial x} + \rho v \frac{\partial h}{\partial y} &= u \frac{\partial p_e}{\partial x} + \frac{\partial}{\partial y}\Big(k \frac{\partial T}{\partial y}\Big) + \mu \Big(\frac{\partial u}{\partial y}\Big)^2
\end{aligned}$$

Here, the gas viscosity and thermal conductivity are given by μ and k. The subscript e denotes the value at the edge of the boundary layer – here p_e is the boundary layer edge pressure and is determined from an inviscid analysis.

In the normalization of the governing equations, we assumed that

$$\frac{1}{\gamma M_1^2} \frac{\partial \bar{p}}{\partial \bar{y}} = \mathcal{O}(1)$$

where the overbar represents the non-dimensional quantities. This assumption is required for the pressure to be uniform across the boundary layer. However, it is not always valid

in hypersonic flows. For example, when a shock impinges on the boundary layer there will be a strong pressure gradient across the boundary layer, and the equations are not valid.

For a well-posed problem, we need boundary conditions. Generally, we assume that the no-slip boundary condition holds, and the velocity on the surface is zero. At high-altitude rarefied conditions, the no-slip boundary condition can fail; under these conditions a more sophisticated boundary condition must be used. We will discuss this as part of the advanced topics later in this section. We also need a boundary condition on enthalpy or temperature – usually we have an isothermal wall such that $T = T_w$ at the surface. A useful limiting condition occurs when there is no heat transfer to the surface; this is the adiabatic wall condition. In this case, $\frac{\partial T}{\partial y}\big|_{y=0} = 0$. The resulting temperature at $y = 0$ is the adiabatic wall temperature, T_{aw}. At the boundary layer edge, the flow state is equal to the edge conditions, obtained from the inviscid analysis: $u = u_e$ and $T = T_e$.

For hypersonic flows, the surface boundary conditions can be much more complicated. For example, there could be conduction into the body and the surface could be hot enough that it radiates away energy. Then the boundary condition would balance the heat transfer rate from the flow to the surface, the heat flux into the body, and the radiative energy flux away from the surface. For reacting flows, the surface can act to catalyze certain reactions, and the change in chemical energy can be deposited at the surface, resulting in increased heating relative to a chemically-inert surface. At planetary entry conditions, the surface is often ablative, which results in chemical reactions and/or phase change at the surface.

Self-Similar Solution of the Boundary Layer Equations

Here we apply the Lees-Dorodnitsyn Transformation to the boundary layer equations. This involves changing the x, y variables to ξ, η through:

$$\xi = \int_0^x \rho_e u_e \mu_e \, dx$$

$$\eta = \frac{u_e}{\sqrt{2\xi}} \int_0^y \rho \, dy$$

We also let:

$$f' = f'(\xi, \eta) = \frac{u}{u_e}, \quad g = g(\xi, \eta) = \frac{h}{h_e}$$

Substituting into the boundary layer equations gives:

$$\big(Cf''\big)' + ff'' = \frac{2\xi}{u_e}\Big[(f')^2 - \frac{\rho}{\rho_e}\Big]\frac{du_e}{d\xi} + 2\xi\Big[f'\frac{\partial f'}{\partial \xi} - f''\frac{\partial f}{\partial \xi}\Big]$$

where:

$$f' = \frac{\partial f}{\partial \eta}, \quad f'' = \frac{\partial^2 f}{\partial \eta^2}, \quad C = \frac{\rho\mu}{\rho_e \mu_e}$$

and the energy equation is:

$$\Big(\frac{C}{Pr}g'\Big)' + fg' = 2\xi\Big[f'\frac{\partial g}{\partial \xi} + \frac{f'g}{h_e}\frac{dh_e}{d\xi} - g'\frac{\partial f}{\partial \xi} + \frac{\rho_e u_e}{\rho h_e}f'\frac{du_e}{d\xi}\Big] - C\frac{u_e}{h_e}\big(f''\big)^2$$

where Pr is the Prandtl number, given by

$$Pr = \frac{\mu c_p}{k}$$

For air, $Pr \simeq 0.72$. The boundary conditions for the above differential equations are:

$$\text{at } \eta = 0 \text{ (wall)},\ f = f' = 0;\ g = g_w \text{ or } g' = 0$$
$$\text{at } \eta \to \infty \text{ (BL edge)},\ f' = 1;\ g = 1$$

Here we have taken $f = 0$ at $y = 0$ for convenience, since only its derivative is relevant to the solution.

Flat Plate or Wedge Boundary Layer Flow

It is not obvious that the above transformed differential equations are easier to solve than the original governing equations. However, if we consider a situation in which the boundary layer edge conditions are constant, then the equations simplify considerably. In this case, all of the ξ derivatives of the edge variables vanish. This flow would correspond to a flat plate boundary layer or to the flow over a wedge with constant post-shock conditions. We also assume that the ξ derivatives of f, g, and their derivatives are zero – we will have to verify that this is a valid assumption.

With these assumptions, the boundary layer equations become:

$$\Big(Cf''\Big)' + ff'' = 0$$
$$\Big(\frac{C}{Pr}g'\Big)' + fg' + C\frac{u_e^2}{h_e}\big(f''\big)^2 = 0$$

Note that these equations are functions of η only, and they are self-similar in η. The boundary conditions remain the same as above. This simplifies the analysis and solution because the problem is now one-dimensional in η.

Now the question is: How to solve these equations? We have a third-order ordinary differential equation in f and a second-order ODE in g. The usual way to solve higher-order ODEs is to convert them to a series of first-order ODEs and then use a method for integrating first-order ODEs. If we let:

$$a = f',\ b = f'' = a',\ c = g'$$

then we obtain the five first-order ODEs:

$$\begin{aligned} f' &= a \\ a' &= b \\ g' &= c \\ Cb' &= -C'b - fb \\ \frac{C}{Pr}c' &= -\frac{C'}{Pr}c - fc - C\frac{u_e^2}{h_e}b^2 \end{aligned}$$

Now we can use our favorite ODE solver – such as fourth-order Runge-Kutta – to integrate these equations.

However, there is a problem: how to enforce the boundary conditions? We have three boundary conditions at the wall ($\eta = 0$) and two at the edge of the boundary layer ($\eta \to \infty$). Thus, we cannot simply start at the wall and integrate out to the edge because we do not have five boundary conditions at the wall. Therefore, we must use an iterative "shooting" method, in which we guess two of the wall conditions, solve to the boundary layer edge, check to see if the solution satisfies $f' = g = 1$ at the edge, and then adjust the guess and "shoot" at the target again until convergence. For example, in the isothermal wall case, we have $f(0)$, $f'(0)$, and $g(0)$; we have to guess $f''(0)$ and $g'(0)$.

This solution method is tedious because we're trying to match two edge conditions with two wall conditions, and the solution is very sensitive to the gradients of f' and g at the wall (corresponding to gradients in u and T). Therefore, this two-variable shooting method is almost impossible to make work by hand. Instead, we can automate the solution using a numerical Newton method. Let us define:

$$\mathcal{F} = \begin{pmatrix} f'(\eta \to \infty) - 1 \\ g(\eta \to \infty) - 1 \end{pmatrix} = \begin{pmatrix} 0 \\ 0 \end{pmatrix}, \quad U = \begin{pmatrix} f''(0) \\ g'(0) \end{pmatrix}$$

The Newton method is then obtained by looping over n with the n^{th} iterate given by:

$$\mathcal{F}^{n+1} = \mathcal{F}^n + \frac{\partial \mathcal{F}}{\partial U}\Delta U$$

where

$$\frac{\partial \mathcal{F}}{\partial U} = \begin{pmatrix} \frac{\partial \mathcal{F}_1}{\partial U_1} & \frac{\partial \mathcal{F}_1}{\partial U_2} \\ \frac{\partial \mathcal{F}_2}{\partial U_1} & \frac{\partial \mathcal{F}_2}{\partial U_2} \end{pmatrix}$$

If we assume that $\mathcal{F}^{n+1}$ solves the equation, then

$$U^{n+1} = U^n - \left(\frac{\partial \mathcal{F}}{\partial U}\right)^{-1}\mathcal{F}^n$$

We have to evaluate $\frac{\partial \mathcal{F}}{\partial U}$ by taking a small perturbation to each guess, solving, and computing the numerical derivative to obtain the full Jacobian matrix.

Note that both C and Pr may vary across the boundary layer. Usually, we assume that Pr is constant and use an expression for μ of the form:

$$\mu = \mu_{\text{ref}} \left(\frac{T}{T_{\text{ref}}} \right)^n$$

which is more accurate at high temperatures than the widely-used Sutherland expression, for example. For air, $n \simeq 0.72$. For a calorically perfect gas, we have $h = c_p T$ and

$$\frac{\mu}{\mu_e} = \left(\frac{T}{T_e} \right)^n = g^n$$

then using the fact that pressure is constant across the boundary layer, we have:

$$C = \frac{\rho\mu}{\rho_e \mu_e} = \frac{p}{RT} \frac{RT_e}{p_e} g^n = \frac{p}{p_e} \frac{T_e}{T} g^n = g^{n-1}$$

Thus, we can replace C with g^{n-1} and solve the system of ODEs.

The integration of the boundary layer is performed on η, which must be converted to physical units. This is done by integrating the expression for η to obtain y. For constant edge conditions, we have:

$$\xi = \rho_e u_e \mu_e \, x$$
$$\eta = \frac{u_e}{\sqrt{2 \rho_e u_e \mu_e x}} \int_0^y \frac{\rho_e}{g} \, dy$$

Therefore,

$$\frac{dy}{d\eta} = y' = \frac{\sqrt{2}\, x}{\sqrt{Re_x}} g$$

which can be integrated along with the boundary layer equations; then the data are plotted versus $\frac{y}{x}\sqrt{Re_x}$.

Figure 8 plots the flat plate boundary layer solution for an isothermal wall with $T_w = T_e$. For the constant edge conditions

$$\eta = \frac{y}{x}\sqrt{Re_x}, \quad Re_x = \frac{\rho_e u_e x}{\mu_e}$$

Thus, for a given value of x and edge conditions, the non-dimensional plot can be converted to physical dimensions. Note that the boundary layer becomes thicker as the edge Mach number increases, and that the temperature overshoot increases significantly. These effects are coupled – the higher temperature increases the viscosity, which causes the boundary

layer thickness to increase. The wall temperature boundary condition has a profound impact on the boundary layer profile, as shown in Figure 9. Note that the adiabatic wall case has a much larger thickness, and the wall temperature is about 18 times the edge temperature.

We can use these solutions to determine the skin friction and heat transfer rate, which is ultimately what we are concerned with. From the boundary layer transformation, we have:

$$c_f = \frac{\tau_w}{\frac{1}{2}\rho_e u_e^2} = \sqrt{2}\frac{\rho_w \mu_w}{\rho_e \mu_e}\frac{f''(0)}{\sqrt{Re_x}}$$

$$C_H = \frac{q_w}{\rho_e u_e (h_{aw} - h_w)} = \frac{1}{\sqrt{2}}\frac{1}{\mu_e}\frac{k_w}{c_{pw}}\frac{\rho_w}{\rho_e}\frac{h_e}{(h_{aw} - h_w)}\frac{g'(0)}{\sqrt{Re_x}}$$

We can then plot $c_f\sqrt{Re_x}$ versus Mach number for the cases plotted above. For the heat transfer coefficient, C_H (also known as the Stanton number), we need the adiabatic wall enthalpy, h_{aw}. This is the enthalpy corresponding to the adiabatic wall temperature (as plotted in Figure 9, for example). We can run the flat plate boundary layer calculation with $g'(0) = 0$ to obtain T_{aw} and h_{aw}. However, we usually use the recovery factor, r, which is defined using:

$$h_{aw} = h_e + r\tfrac{1}{2}u_e^2$$

$$h_o = h_e + \tfrac{1}{2}u_e^2$$

$$h_{aw} = h_e + r(h_o - h_e)$$

or:

$$r = \frac{h_{aw} - h_e}{h_o - h_e} = \frac{T_{aw} - T_e}{T_o - T_e}$$

from the solution of the boundary layer equations, it can be shown that $r \simeq \sqrt{Pr}$. With this result, we can also plot $C_H\sqrt{Re_x}$ as a function of edge Mach number and wall temperature.

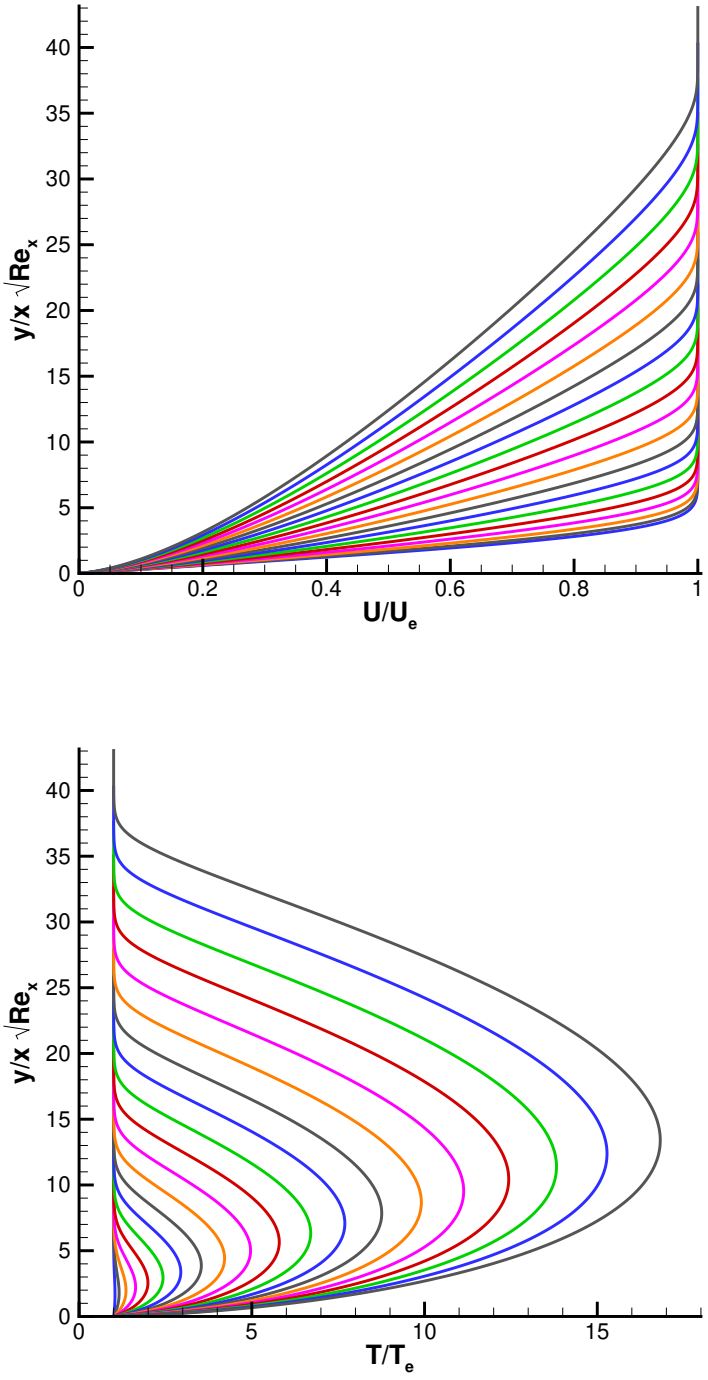

Figure 8. Flat plate boundary layers with $T_w/T_e = 1$; edge Mach number ranges from 1 to 20.

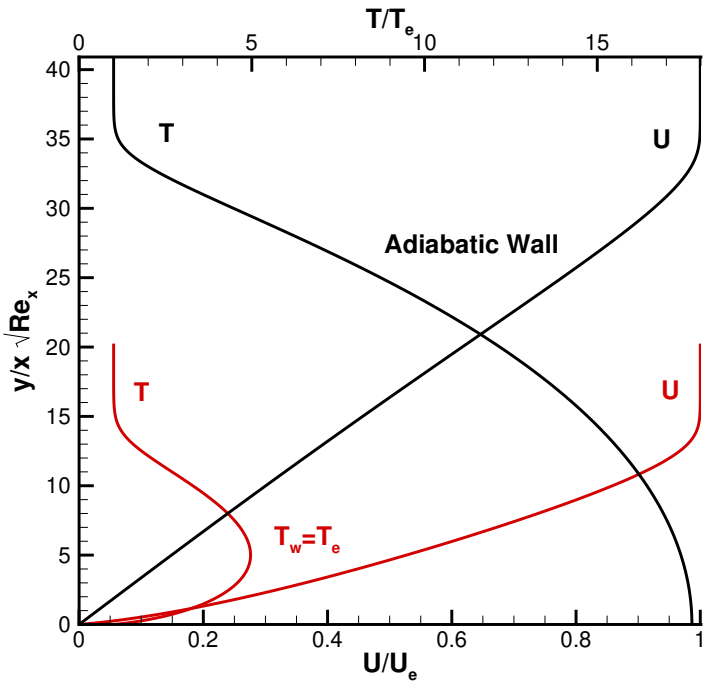

Figure 9. Flat plate boundary layers with edge Mach number of 10 and cold wall and adiabatic wall boundary conditions.

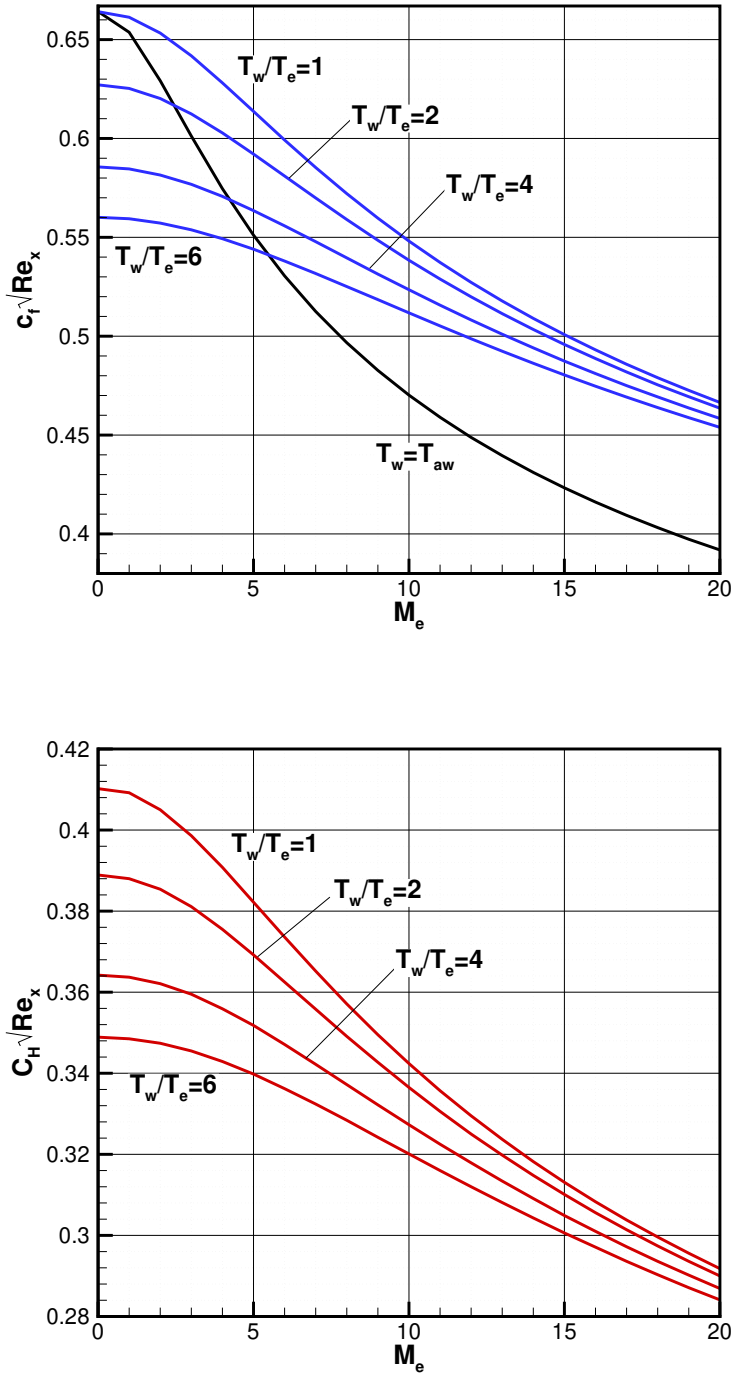

Figure 10. Skin friction and heat transfer coefficients as a function of edge Mach number and wall cooling for the flat plate boundary layer.

To use these results, we compute the edge conditions and then read off the values for $c_f\sqrt{Re_x}$ and $C_H\sqrt{Re_x}$; then for the given Re_x and h_{aw}, we can compute the skin friction and heat flux. For example, let us compute the heat flux to a flat plate flying at $\alpha = 0$, $M = 10$, and 30 km altitude; assume $T_w = T_e$.

The edge conditions are the free-stream conditions: $\rho_e = 0.0180\,\mathrm{kg/m^3}$, $u_e = 3018\,\mathrm{m/s}$, $T_e = 226.7\,\mathrm{K}$. With the Sutherland expression for viscosity, we have: $\mu_e = 1.458 \times 10^{-6}\sqrt{T_e^3}/(T_e + 110.3) = 1.48 \times 10^{-5}\,\mathrm{kg/m\,s}$, and $Re_x/x = 3.67 \times 10^6$. From Figure 10, we have:

$$c_f\sqrt{Re_x} = 0.548, \quad C_H\sqrt{Re_x} = 0.342$$

Also, we can compute $h_{aw} = 4.09 \times 10^6\,\mathrm{J/kg}$. Then the shear stress and heat flux are:

$$\tau_w = \frac{1}{2}\rho_e u_e^2\, c_f = \frac{23.4}{\sqrt{x}}\,\mathrm{Pa}$$

$$q_w = \rho_e u_e^2 (h_{aw} - h_w)\, C_H = \frac{37,500}{\sqrt{x}}\,\mathrm{W/m^2}$$

Note that the skin friction and heat flux are singular at the plate leading edge because the boundary layer has zero thickness there. This is clearly aphysical, and in reality, rarefaction effects will reduce these quantities near the leading edge.

A word about units: the MKS heat flux unit is $\mathrm{W/m^2}$, which is cumbersome and therefore is seldom used. It is common to express heat flux in units of $\mathrm{W/cm^2}$, because this has a more convenient range of values. Thus, the heat flux computed above would usually be expressed as $3.7/\sqrt{x}\,\mathrm{W/cm^2}$. Now, is this a large value or not? The solar flux is about $0.1\,\mathrm{W/cm^2}$ and a toaster produces about $1\,\mathrm{W/cm^2}$; the Shuttle Orbiter peak stagnation point heat flux was about $30\,\mathrm{W/cm^2}$, and Apollo entry peak heating was about $200\,\mathrm{W/cm^2}$.

From Figure 10, we see that c_f and C_H decrease with increasing wall temperature. They also decrease with increasing M_e. This makes sense in light of Figures 8 and 9, because higher boundary layer temperatures increase the boundary layer thickness, resulting in smaller velocity and temperature gradients at the wall. Thus, we see that:

1. δ increases with M_e
2. T increases with M_e
3. wall cooling decreases δ
4. c_f and C_H decrease with M_e
5. c_f and C_H increase with wall cooling

Of course, c_f and C_H are non-dimensional, so the actual skin friction and heat flux values depend on the edge conditions.

The boundary layer solution discussed above is easily modified to make it apply to axisymmetric (cone) flows. This is the Mangler transformation, and the main result is that the results presented in Figure 10 above can be applied to cones by multiplying the coefficients by a factor of $\sqrt{3}$.

Also, Reynolds Analogy is often used to relate the skin friction to the heat transfer rate coefficient through

$$\frac{C_H}{c_f} \simeq \tfrac{1}{2} Pr^{-2/3}$$

This is often used in hypersonic experiments to relate heat flux measurements (easy) to skin friction (difficult).

Stagnation Point Heat Transfer Rate

Now let us consider the boundary layer flow at the stagnation point of a hypersonic vehicle. This is often the location of maximum heating, and therefore it is important to predict. Here, the edge conditions vary in the x direction around the body; the velocity and pressure gradients are non-zero. The boundary layer equations for this case are:

$$\big(Cf''\big)' + ff'' = \frac{2\xi}{u_e}\Big[(f')^2 - \frac{\rho_e}{\rho}\Big]\frac{du_e}{d\xi}$$
$$\Big(\frac{C}{Pr}g'\Big)' + fg' = 2\xi\Big[\frac{f'g}{h_e}\frac{dh_e}{d\xi} + \frac{\rho_e u_e}{\rho h_e}f'\frac{du_e}{d\xi}\Big] - C\frac{u_e}{h_e}\big(f''\big)^2$$

For the stagnation point flow $u_e^2 \ll h_e$, and we can write the edge velocity as the first term in a Taylor series as:

$$u_e \simeq \frac{du_e}{dx}\Big|_s x$$

since $u_e = 0$ at $x = 0$, where the s subscript denotes the stagnation point. Then from the definition of ξ, we have:

$$\xi = \int_0^x \rho_e u_e \mu_e \, dx \simeq \rho_e \mu_e \int_0^x u_e \, dx$$

We can integrate this expression to obtain

$$\xi = \rho_e \mu_e \frac{x^2}{2}\frac{du_e}{dx}\Big|_s = \rho_e \mu_e u_e \frac{x}{2}$$

Then we can show that $\frac{2\xi}{x}\frac{dx}{d\xi} = 1$, and the right-hand side of the momentum equation reduces to $\big((f')^2 - g\big)$. Similar algebra can be done for the energy equation, and if we

use the fact that $h_o = h_e = \frac{1}{2}u_e^2$ is constant, we can show that the right-hand side of the energy equation reduces to zero.

Therefore, we obtain the final form of the stagnation point boundary layer equations:

$$\begin{aligned}\left(Cf''\right)' + ff'' &= \left(f'\right)^2 - g \\ \left(\frac{C}{Pr}g'\right)' + fg' &= 0\end{aligned}$$

which we solve in the same way as before.

Note that the only scaling has to do with $\frac{du_e}{dx}$, which determines the magnitude of the right-hand side of the momentum equation. Namely,

$$\frac{2\xi}{x}\frac{dx}{d\xi} = 1$$

Also, the wall temperature enters through the boundary condition. It is a simple matter to write down the five first-order ODEs, and then solve with the same type of iterative shooting method. Note that $g_w = T_w/T_e$ is the only parameter that we can vary for this problem.

Once we have solved the boundary layer equations, we have to compute the heat flux, $q_w = -k\frac{\partial T}{\partial y}\big|_w$. We use the definition of η to obtain:

$$\frac{\partial T}{\partial y}\Big|_w = \frac{dT}{d\eta}\frac{\partial \eta}{\partial y}\Big|_{\eta=0} = T_e g'(0)\rho\frac{u_e}{\sqrt{2\xi}}$$

with the expression for u_e and ξ above, we have:

$$q = \frac{\rho_w\mu_w}{\sqrt{\rho_e\mu_e}}\frac{1}{Pr}\sqrt{\frac{du_e}{dx}}h_e\, g'(0)$$

From the boundary layer solution, we can obtain $g'(0)$ as a function of $\frac{T_w}{T_e}$; Figure 11 plots this quantity. Note that μ_w and ρ_w are functions of T_w, so the maximum in $g'(0)$ does not imply a maximum in q_w.

Van Driest (1956) solved these equations and obtained a correlation for $g'(0)$. This is written as:

$$q_w = \kappa Pr^{-0.6}\sqrt{\rho_e\mu_e}\sqrt{\frac{du_e}{dx}\big|_s}\left(h_{aw} - h_w\right)$$

where $\kappa = 0.57$ for a cylinder and $\kappa = 0.763$ for a sphere; comparing with the boundary layer solution shows that this expression is remarkably accurate and is valid to $\pm 0.5\%$.

Now we need to evaluate the stagnation point edge velocity gradient, $\frac{du_e}{dx}\big|_s$. To do so, we use the Euler equation that relates pressure gradients to velocity gradients through:

$$dp_e = -\rho_e u_e \, du_e$$

and Newtonian aerodynamics

$$C_p = 2\sin^2\delta = 2\cos^2\phi = \frac{p_e - p_1}{\frac{1}{2}\rho_1 V_1^2}$$

where ϕ is $\frac{\pi}{2} - \delta$. Differentiating this expression yields

$$\frac{dp_e}{dx} = -2\rho_1 V_1^2 \cos\phi \sin\phi \frac{d\phi}{dx}$$

It is easy to show that

$$\frac{d\phi}{dx} = \frac{1}{R_n}$$

where R_n is the nose radius of the vehicle at the stagnation point. Then using the expression for u_e, we obtain:

$$\frac{du_e}{dx}\big|_s = \frac{1}{R_n}\sqrt{\frac{2(p_e - p_1)}{\rho_e}}$$

Thus, the final result for the stagnation point boundary layer heat transfer rate is simply:

$$q_w = \kappa Pr^{-0.6}\sqrt{\rho_e \mu_e}\frac{1}{\sqrt{R_n}}\Big(\frac{2(p_e - p_1)}{\rho_e}\Big)^{1/4}\big(h_{aw} - h_w\big)$$

This is one of the most important results in hypersonic aerodynamics because it is accurately represents a critical quantity with a simple expression.

Note that the heat flux scales inversely with the square root of the vehicle nose radius. Thus, the nose radius (bluntness) of a vehicle can be increased in order to reduce the stagnation point heat flux. This is why hypersonic vehicles have blunted leading edges and why large blunt capsules are used for planetary entry missions.

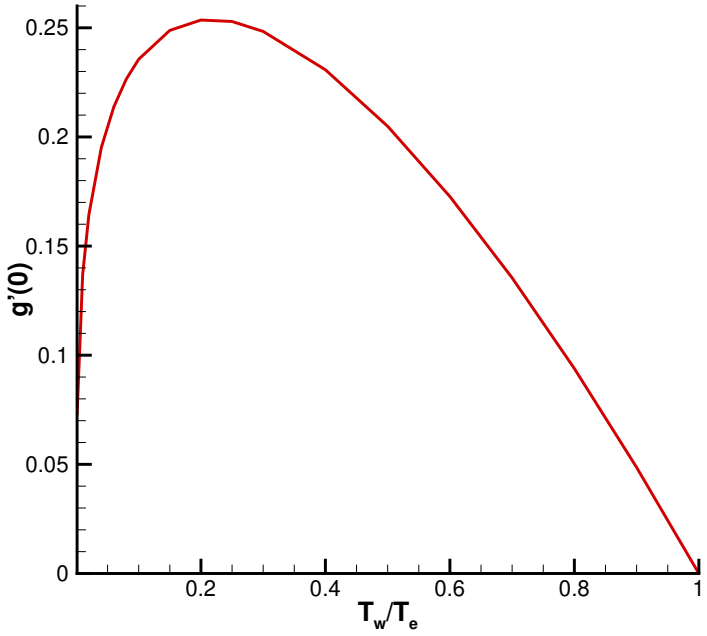

Figure 11. Variation of the non-dimensional temperature gradient, $g'(0)$ with wall temperature for the stagnation point boundary layer flow.

We can do a simple example to illustrate the use of the stagnation point heat transfer rate formula. Take $\rho_1 = 0.01\,\mathrm{kg/m^3}$, $T_1 = 227\,\mathrm{K}$, $u_1 = 3000\,\mathrm{m/s}$, and $T_w = 1000\,\mathrm{K}$. Assume that this represents the cylindrical leading edge of a hypersonic vehicle, with radius 1 cm. Using perfect gas tables, we obtain the boundary layer edge conditions (also for this case, the inviscid stagnation point conditions) of:

$$p_e = p_O = 129.22\,p_1 = 84200\,\mathrm{Pa}; \quad T_e = T_o = 4770\,\mathrm{K}; \quad \rho_e = \rho_o = 0.0615\,\mathrm{kg/m^3}$$

the adiabatic wall enthalpy is the total enthalpy. Then with

$$\mu_e = \mu_{\mathrm{ref}}\left(\frac{T}{T_{\mathrm{ref}}}\right)^{0.72} = 1.478\times10^{-5}\left(\frac{4770}{227}\right)^{0.72} = 1.32\times10^{-4}\mathrm{kg/m\,s}$$

This then yields:

$$q_{w,\mathrm{cyl}} = 304\,\mathrm{W/cm^2}$$

Boundary Layer with Chemical Reactions

Now let us consider extending the boundary layer equations to include the effects of chemical reactions and energy transport across the boundary layer and to the vehicle surface. The heat flux includes and energy transport term due to the mass diffusion of chemical species. Thus,

$$q_w = -k\frac{\partial T}{\partial y}\Big|_w + \sum_s \left(\rho_s v_s h_s\right)_w$$

where v_s is the diffusion velocity of species s in the y direction and h_s is the enthalpy per unit mass of that species. In a mixture of gases, each species may have its own velocity, which may be different than the average (or bulk) velocity. This is because the gas species diffuse relative to one another driven by variations in species concentrations and boundary conditions. A simple model for the species s diffusion flux is Fick's law, which assumes the flux is proportional to mass fraction gradients:

$$\rho_s v_s = -\rho D\frac{\partial c_s}{\partial y}$$

The contribution to the heat flux is due to each species carrying its energy with it as it diffuses. Note that this is a different energy transport term than the usual $k\frac{\partial T}{\partial y}$ term – note that we can have energy flux with a zero temperature gradient. In air, the main component of the diffusive energy flux is usually due to the heat of formation of the atomic species. For example, consider a mixture of N_2 and N; from the previous analysis, we have:

$$h_{N_2} = \frac{7}{2}\frac{\hat{R}}{M_{N_2}}T + \frac{\hat{R}}{M_{N_2}}\frac{\theta_{v,N_2}}{e^{\theta_{v,N_2}/T}-1}$$

$$h_N = \frac{5}{2}\frac{\hat{R}}{M_{N_2}}T + h_N^\circ$$

Here, h_s° is the heat of formation of species s; $h_N^\circ = 33.62\,\mathrm{MJ/kg}$ and $h_O^\circ = 15.42\,\mathrm{MJ/kg}$. These are obviously very large values.

Let us consider a case where there is diffusive energy transport to a surface for this two-species gas mixture. Since the sum of the mass fractions is one, the gradients of the two species are opposite one another:

$$\frac{\partial c_{N_2}}{\partial y} = -\frac{\partial c_N}{\partial y}$$

and the diffusive part of energy flux at the wall is:

$$q_{w,\mathrm{diff}} = \rho D\left(h_{w,N} - h_{w,N_2}\right)\frac{\partial c_N}{\partial y}$$

The thermal parts of the species enthalpies approximately cancel with each other, and:

$$q_{w,\text{diff}} \simeq \rho D h^\circ_{\text{N}} \frac{\partial c_{\text{N}}}{\partial y}$$

Thus, there is a heat flux to the surface due to gradients in the chemical species and the diffusive mass flux carrying chemical energy to the surface.

The transport of chemical energy to the surface may be caused by one of two processes:

1. The vehicle surface material catalyzes the nitrogen recombination reaction: $2\text{N} \rightarrow \text{N}_2$. In this case, the surface N mass fraction is small due to efficient surface recombination – thus, the boundary condition of the N atom species mass fraction has small (or zero) c_{N} at the wall.
2. The nitrogen recombines in the boundary layer due to recombination in the low-temperature and high-density region near a cold wall. This causes the recombination reaction to take place in the gas phase, resulting in low values of c_{N} near the wall and a c_{N} gradient.

Note that if the wall is inert so that it does not catalyze recombination at the wall and the recombination reaction is slow in the boundary layer, then the gradient of c_{N} near the wall could be small. Then the diffusive transport of chemical energy would be reduced.

Similar to the Prandtl number, we define the Lewis number which is the ratio of the mass diffusivity to the thermal diffusivity (for air, $Le \simeq 1.4$).

$$Le = \frac{\rho D c_p}{k}$$

Fay and Riddell (1957) solved the boundary layer equations with dissociated air; the analysis is similar to the stagnation point analysis, but there is now an equation for the variation of the chemical state across the boundary layer. They analyzed three limiting cases, corresponding to the energy transport discussion above. These are:

1. Chemical equilibrium boundary layer: the reaction rates are very fast relative to the gas motion and adjust immediately to the temperature in the boundary layer.
2. Chemically frozen boundary layer with a fully catalytic surface: the reaction rates are very slow (chemical state remains frozen at the edge condition), and the surface promotes recombination at the wall due to catalytic processes. Thus all of the dissociated gas recombines at the wall.
3. Chemically frozen boundary layer with a non-catalytic surface: the reactions are frozen and the wall is inert, so that it does not catalyze recombination at the surface.

The Fay and Riddell results for these limiting cases are:

$$q_w = \kappa Pr^{-0.6}\left(\rho_e\mu_e\right)^{0.4}\left(\rho_w\mu_w\right)^{0.1}\sqrt{\left.\frac{du_e}{dx}\right|_s}\left(h_o - h_w\right) \times F$$

F is a factor that varies with the three cases above:

$$F = \begin{cases} 1 + \left(Le^{0.52} - 1\right)\frac{h_D}{h_o}, & \text{Case 1;} \\ 1 + \left(Le^{0.63} - 1\right)\frac{h_D}{h_o}, & \text{Case 2;} \\ 1 - \frac{h_D}{h_o}, & \text{Case 3} \end{cases}$$

where h_D is the enthalpy stored in dissociation at the boundary layer edge:

$$h_D = \sum_s c_{se} h_s^\circ$$

Note that since $Le \simeq 1.4$, Case 2 has a slightly larger value than Case 1; and Case 3 with no gas-phase or gas-surface recombination can produce a much lower value of heat transfer rate. The energy stored in dissociation is not returned to the vehicle surface, reducing the heat flux.

It may seem strange that there could be significant levels of dissociation in the inviscid region of the flow, yet have a chemically frozen boundary layer. This effect is caused by the scaling of the reaction processes with density. Dissociation is a binary reaction, involving the collision of a diatomic molecule and another particle: $N_2 + M \rightarrow N + N + M$ for nitrogen. Recombination requires the two N atoms to collide in the presence of a third particle so that the energy released by the bond formation can be carried away. Thus, the dissociation process has binary scaling flow density, but the recombination process has ternary scaling. Thus, under certain hypersonic conditions, it is possible to have significant levels of dissociation with minimal levels of recombination in the boundary layer.

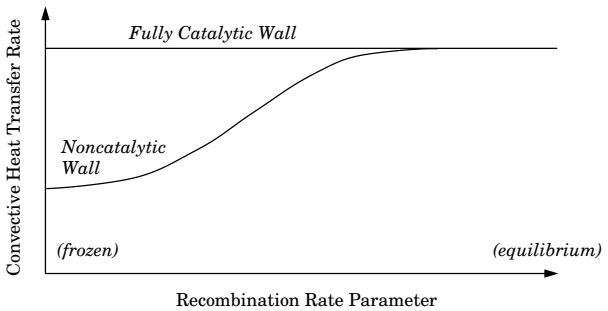

Figure 12. Variation of stagnation point heat flux with recombination rate and wall catalysis.

Figure 12 (taken from Fay and Riddell) shows how the stagnation point heat flux varies with the gas-phase recombination rate for the two limiting values of wall catalysis. Note that for a fully catalytic surface the heat flux is independent of reaction rate, while the potential benefits of a non-catalytic surface diminish as the rate of recombination increases. Clearly, a partially catalytic surface would fall between the limits shown here.

Most thermal protection materials (TPS) are designed to be nearly non-catalytic to exploit this effect. For example, the RCG (reaction-cured glass) coating on the Shuttle tiles is nearly non-catalytic. At the time of the design of the Shuttle, it was known that there could be a reduction in heat flux due to slow recombination in boundary layer and low levels of catalytic efficiency of the tiles. However, the TPS was designed assuming that the flow field would be in chemical equilibrium everywhere[1] (Fay and Riddell Case 1). As expected, the surface temperatures measured in flight were lower than the predicted levels.

To study the effect of catalytic surfaces at flight conditions, data were taken on modified tiles during Shuttle flights STS-2 through STS-5. Several tiles were coated with a highly catalytic material and the thermocouples were used to measure the near-surface temperature. The flight data showed that the catalytic tiles had significantly larger temperatures than the uncoated tiles. Figure 13 shows an image taken from this study. Here, the normalized surface temperature is plotted other data indicate that the heat flux essentially doubled due to the catalytic coating.

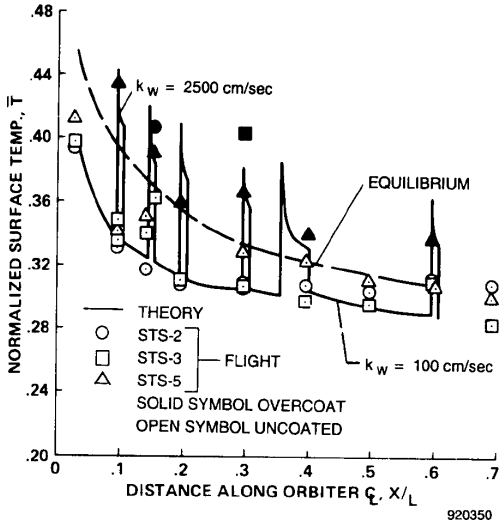

Figure 13. Normalized Shuttle surface temperature on the windward centerline, showing effect of catalytic tile coating.

[1] K.W. Iliff and M.F. Shafer, "Space Shuttle Hypersonic Aerodynamic and Aerothermodynamic Flight Research and Comparison to Ground Test Results," NASA TM-4499, June 1993.

Boundary Condition for a Catalytic Surface

In the Fay and Riddell analysis, the limiting values of wall catalysis were used. Here, we consider how to represent the situation when the surface is partially catalytic. We define the catalytic efficiency, α, as the fraction of particles hitting the surface that recombine on the surface. The flux of species s particles to the surface can be determined from kinetic theory of gases as:

$$\left(\rho_s v_s\right)_w = \frac{\rho_{sw}}{4}\sqrt{\frac{8\hat{R}T_w}{\pi M_s}}$$

This is obtained by integrating the velocity distribution function to obtain the one-way flux of particles across an arbitrary surface.

This result can be used to determine the gas state at the surface as a function of α and the gas properties. For example, consider a two species gas composed of O_2 and O. The flux of O atoms to the surface is

$$\left(\rho_{\mathrm{O}} v_{\mathrm{O}}\right)_w = \frac{\rho_{\mathrm{O}w}}{4}\sqrt{\frac{8\hat{R}T_w}{\pi M_{\mathrm{O}}}}$$

of this, α_{O} react and $(1-\alpha_{\mathrm{O}})$ reflect off of the surface. Thus, there is a flux of recombined O_2 molecules from the surface:

$$\left(\rho_{\mathrm{O}_2} v_{\mathrm{O}_2}\right)_w = \frac{\alpha_{\mathrm{O}}\rho_{\mathrm{O}w}}{4}\sqrt{\frac{8\hat{R}T_w}{\pi M_{\mathrm{O}}}} = \rho_w D_{\mathrm{O}_2}\frac{\partial c_{\mathrm{O}_2}}{\partial y}\Big|_w$$

Thus, it is possible to determine the wall mass fraction of O_2 and O that produces this flux. This sets the boundary condition for the species mass conservation equations.

In practice, the catalytic efficiency is difficult to measure precisely and can be highly variable depending on the detailed microstructure of the surface – how many open bond sites are available, and how particles interact with those sites. In reality, the surface reaction process is more complicated than just a single catalytic efficiency, and may involve temperature-dependent mechanisms. For example, Figure 14 plots the nitrogen and oxygen atom catalytic efficiency for the reaction-cured glass (RCG) coating that was used for the Shuttle tiles. This plot is taken from the work of Stewart, which involved measurements in different facilities to infer the catalytic efficiency. Note that at all temperatures, the catalytic efficiency is quite low (less than about 0.01) and that there are large variations as a function of temperature. Presumably, there are physical gas-surface interaction mechanisms behind this variation.

Finally, it is important to recognize that the above boundary condition has a limit when $\alpha = 1$, which implies that every atom that diffuses to the surface recombines on the

surface – this corresponds to a fully catalytic surface. However, this does not necessarily imply that the mass fraction of atomic species is zero on the surface. This can be seen in the above equation for the mass fraction gradient at the wall; this boundary condition gives the slope of the mass fraction, but not the value of the mass fraction. Thus, there can be atomic species near the surface even when the surface is fully catalytic – the diffusive mass flux limits the transport rate of those species to the surface, effectively limiting the rate at which the surface can catalyze the recombination.

In some analyses, a so-called "super-catalytic" wall boundary condition is used, in which the mass fraction of atomic species is set to zero on the surface. This is not a physical boundary condition, because it is not consistent with the flux-based boundary condition described above.

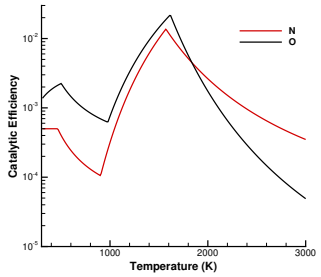

Figure 14. RCG catalytic efficiency from the work of Stewart.

Laminar-Turbulent Transition

The discussion and results obtained so far have been for laminar boundary layers. For many hypersonic vehicles, the flow field will be laminar for a portion of the trajectory, and then transition to turbulent flow. The heat flux and skin friction increase dramatically – by roughly a factor of 5 – when the flow transitions from a laminar to a turbulent state. In a laminar boundary layer, transport occurs due to molecular diffusion, whereas in a turbulent boundary layer tranport is caused by a huge number of vortices that convectively mix the flow. This process is much more efficient than molecular diffusion, resulting in larger gradients at the surface.

Because heat transfer rate and the total heat load (integral of heat flux along the vehicle's trajectory) are design drivers, it is critical to determine when the flow transitions from laminar to turbulent flow. We will see that the Shuttle Orbiter re-entry trajectory was carefully designed to avoid transition to turbulence until late in the trajectory. If transition occurred near the maximum heating point of the trajectory, it would have been possible to overheat the tiles and cause failure of the thermal protection system.

It is not possible to provide a detailed description of the transition process in these notes; an entire course could be given on this topic, and it is currently the subject of active research. The best source for additional details are a series of review papers written by Prof. Steven Schneider.

In hypersonic flows, laminar-turbulent transition is though to occur as a result of several physical mechanisms. For example, consider the boundary layer on a cone at zero angle of attack in hypersonic flow. If an acoustic disturbance enters the boundary layer (due to free-stream noise, for example), the boundary layer may amplify the disturbance. This occurs if the disturbance reflects between the cone surface and the disturbance's sonic point in the boundary layer. Thus, if the disturbance has a frequency that is tuned to the boundary layer, the boundary layer can act like a wave guide and the disturbance will draw energy from the flow. If there is a sufficient region of amplification, the disturbance will cause the flow to become unstable and breakdown to turbulent flow.

Stability theory has been shown to be effective at predicting transition for boundary layers that are susceptible to this acoustic instability mechanism. The basic approach is to linearize the Navier-Stokes equations; a disturbance with a particular form is then introduced, resulting in an eigenvalue problem. Candidate disturbances are introduced and their amplification rate is computed, using the laminar flow to provide forcing to the disturbances. Each disturbance is integrated as it flows through the boundary layer, and the cumulative amplification is computed. When a particular disturbance growth reaches a given threshold, the boundary layer is assumed to have become critically unstable. Figure 15 plots the results of such a stability analysis for a blunted 7° cone at free-stream conditions between about Mach 6 and 7. Here, the predicted transition location is plotted versus the measured location (using the location where the heat flux deviates from the laminar value). Here, it is assumed that transition occurs when the most unstable disturbance has grown by a factor of e^N, it has become critical; N must be determined by comparison to experimental data. Here, we use $N = 5.5$, which is a typical value for conventional hypersonic blow-down wind-tunnels that have fairly noisy free-stream flow. The N factor is usually found to be larger for flight where the free-stream has lower levels of noise. In any case, the stability analysis correlates the data very well, showing that this mechanism-based analysis approach shows promise for predicting transition. Research is continuing to apply the methodology to more complex three-dimensional flows.

There are other possible mechanisms that can cause transition to turbulence at hypersonic conditions. Probably the most pervasive source for transition on flight vehicles is discrete roughness due to joints and gaps in the thermal protection system, as well as inher-

ent distributed roughness due to the material itself. The rough surface provides a source of large-amplitude disturbances (relative to those in the free-stream or other sources).

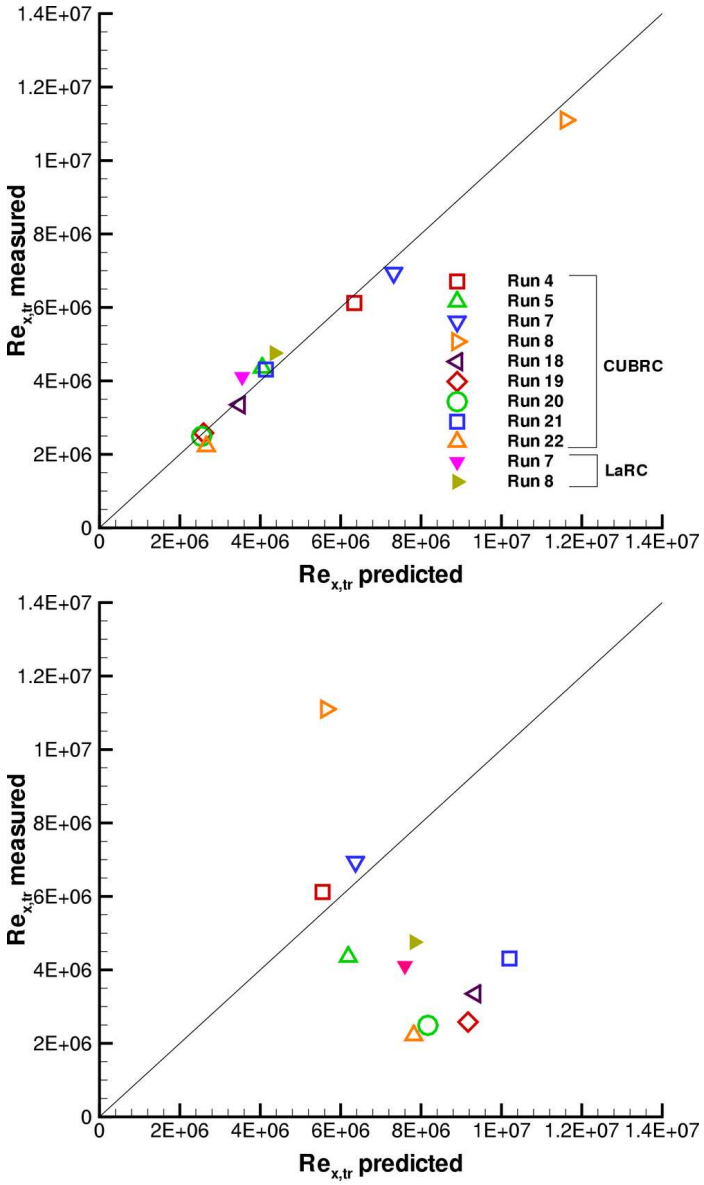

Figure 15. Predicted transition location on the HIFiRE-1 blunted 7° cone at CUBRC and NASA Langley wind-tunnel conditions; e^N mechanism-based approach (top) and Re_θ/M_e correlation approach (bottom).

Estimation of Transition Location

It is not possible to precisely predict transition with simple methods for all flow conditions. This is because for any given free-stream condition, geometry, surface state, and other variables, transition will occur due to a particular mechanism. Thus, correlations to flight and wind-tunnel data are often used to estimate when transition will occur; clearly

this estimate should only be used within the validity of the correlation.

One of the most widely used correlations for estimating transition for hypersonic flows is the ratio of the boundary layer momentum thickness Reynolds number to the edge Mach number. Typically, the location at which the momentum thickness reaches at critical value is taken as the point at which the boundary layer transitions. We write this as:

$$\frac{Re_{\theta,tr}}{M_e} = C^*$$

where C^* is taken as a constant for a class of flow. For example, a commonly used correlation for small bluntness wedges has $C^* \simeq 300$, and for cones $C^* \simeq 150$. Here,

$$Re_{\theta,tr} = \frac{\rho_e u_e \theta_{tr}}{\mu_e}, \qquad \theta = \int_0^y \frac{\rho u}{\rho_e u_e}\Big(1 - \frac{u}{u_e}\Big)\, dy$$

We can represent the momentum thickness in terms of the boundary layer similarity variables as:

$$\theta = \frac{x}{\sqrt{Re_x}}\sqrt{2}\int_0^\infty f'\big(1 - f'\big)\, d\eta$$

and we can integrate this expression across the boundary layer to obtain θ as a function of x and Re_x. For simplicity, let us define ϕ as the integral in the above expression:

$$\phi = \int_0^\infty f'\big(1 - f'\big)\, d\eta$$

and we can plot its value for a range of edge Mach numbers and wall temperatures. Figure 16 plots ϕ for $T_w/T_e = 1$.

Now we can compute the location at which the correlation predicts transition to occur. With some simple algebra, we obtain

$$x_{tr} \simeq \frac{\mu_e}{2\rho_e u_e}\Big(\frac{C^* M_e}{\phi}\Big)^2$$

Note that $\rho_e u_e/\mu_e$ is the unit Reynolds number (Re per unit length), and thus the correlation scales transition with its inverse. Also, with the transition location is predicted to scale with the square of the edge Mach number; the scaling is stronger than quadratic because ϕ decreases with M_e.

Written in a different form, the Re_θ/M_e correlation is

$$x_{tr} = \frac{\theta\sqrt{Re_x}}{\sqrt{2}\phi}$$

and thus the transition location is proportional to the square root of the Reynolds number and the momentum thickness. However, θ is a slowly varying function of x, and thus this correlation approach tends to collapse the data. That is, it reduces the variation in the data, making it appear that the correlation is more accurate than it really is. An example of the Re_θ/M_e correlation is given in Figure 15, showing that for the HIFiRE-1 blunt cone, it is a rather poor predictor of the measured transition location.

Unfortunately, there are few, if any, better correlations available. This is because the transition process depends on many details: M_e, Re, nose bluntness, geometry, wall cooling, facility noise, surface roughness, ablation, free-stream disturbance levels, etc. It is overly optimistic to think that a single correlation could represent the effects of all of these variables.

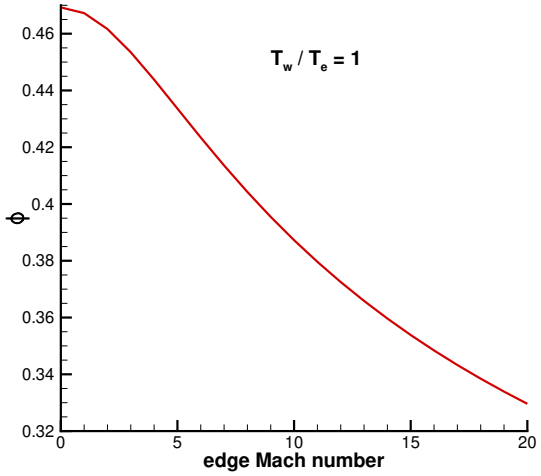

Figure 16. Variation of ϕ with edge Mach number for $T_w/T_e = 1$.

Reference Temperature Method

This is an approximate method in which boundary layer results from incompressible flow are used to evaluate skin friction and heat flux at compressible conditions. The incompressible c_f and C_H are evaluated at "reference" conditions which characterize the average state of the compressible boundary layer. This method is often used in so-called engineering analyses to obtain approximate estimates.

The incompressible flat plate laminar boundary layer solution gives:

$$c_f = \frac{0.664}{\sqrt{Re_x}}, \qquad C_H = \frac{0.332}{\sqrt{Re_x}} Pr^{-2/3}$$

To apply the reference temperature approach, we evaluate Re_x and Pr at the reference

conditions (denoted by a $*$ superscript):

$$c_f = \frac{0.664}{\sqrt{Re_x^*}}, \qquad C_H = \frac{0.332}{\sqrt{Re_x^*}} Pr^{*-2/3}$$

where

$$Re_x^* = \frac{\rho^* u_e x}{\mu^*}, \qquad Pr^* = \frac{\mu^* c_p^*}{k^*}$$

The reference state is obtained from an estimate of the average boundary layer temperature and the condition of constant pressure in the boundary layer.

In the case of a turbulent boundary layer, there are a variety of approximate expressions for the skin friction and heat flux. For example:

$$c_f = \frac{0.02296}{(Re_x^*)^{0.139}}, \qquad C_H = \frac{1}{2} c_f {Pr_t}^{-2/3}$$

where Pr_t is the turbulent Prandtl number.

To obtain the reference conditions, we can use expressions obtained by Meador and Smart. For laminar flow they obtained:

$$\frac{T^*}{T_e} = 0.45 + 0.55\frac{T_w}{T_e} + 0.16r\frac{\gamma - 1}{2} M_e^2$$

where $r = \sqrt{Pr^*}$ is the recovery factor. For turbulent boundary layers their fit is slightly different:

$$\frac{T^*}{T_e} = 0.50 + 0.50\frac{T_w}{T_e} + 0.16r\frac{\gamma - 1}{2} M_e^2$$

where $r = \sqrt[3]{Pr_t}$, and the turbulent Prandtl number is used ($Pr_t = 0.9251$ in their analysis). Note that Meador and Smith used the above correlation for c_f to obtain the fit for the reference temperature. Other correlations would produce different expressions for T^*.

Again, for conical boundary layers, we usually account for the thinner boundary layer by multiplying the above two-dimensional results by a factor of $\sqrt{3}$.

Hypersonic Viscous Interactions

As we have discussed several times, hypersonic flow fields may have a coupling between the viscous and inviscid flow. So far, we have neglected this effect and assumed that the inviscid flow sets the boundary layer edge conditions for the boundary layer analysis. Under certain low Reynolds number and high Mach number conditions, the viscous flow can change the inviscid flow resulting in variations in the surface pressure. The simplest example of this type of viscous-invicid interaction is a flat plate flying at zero angle of

attack. Figure 17 plots the CFD solution for a Mach 10 free-stream at a Reynolds number of 284,000 based on the length of the plate. An adiabatic wall and an isothermal wall ($T_w/T_e = 2$) surface boundary condition is used.

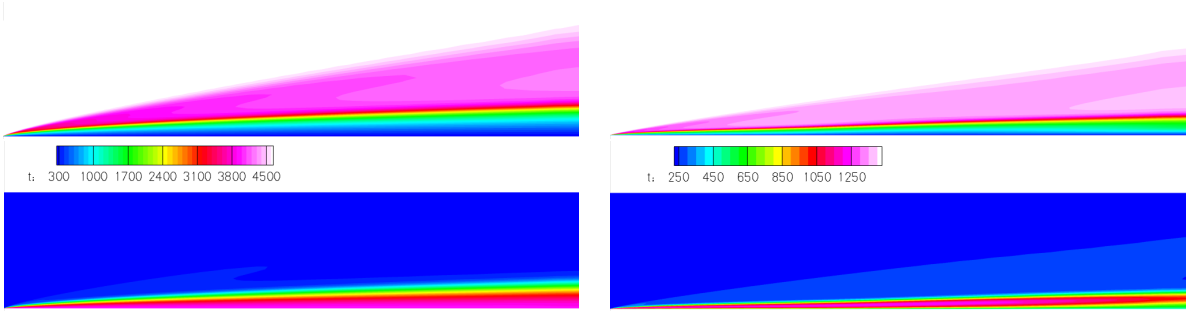

Figure 17. Mach number (top) and temperature distributions (bottom) for a zero angle of attack plate at Mach 10; adiabatic wall (left), isothermal wall (right).

Note that the boundary layer displaces the inviscid flow, which causes a shock wave to form, which modifies the edge conditions. This viscous-inviscid interaction is stronger for the adiabatic wall case because the boundary layer thickness is larger. Thus the boundary layer makes the body appear to have an effective shape, which is given by the boundary layer displacement thickness, δ^*. We will define a strong viscous interaction when the boundary layer growth rate strongly affects the inviscid flow ($d\delta^*/dx$ is large); this will occur near the leading edge, especially for hot-wall cases. A weak viscous interaction occurs where the boundary layer is growing more slowly, and the inviscid flow is weakly affected by the change in the displacement thickness.

Let us compute the variation of the pressure distribution on a flat plate at zero angle of attack in a hypersonic stream. The boundary layer displacement thickness is proportional to x and inversely proportional to the square root of Re_x:

$$\delta^* \propto x\sqrt{\frac{\mu^*}{\rho^* u_1 x}} = x\sqrt{\frac{\mu_1}{\rho_1 u_1 x}}\sqrt{\frac{\rho_1 \mu^*}{\rho^* \mu_1}} = \frac{x}{\sqrt{Re_{1,x}}}\sqrt{\frac{\rho_1 \mu^*}{\rho^* \mu_1}}$$

Now, we use the fact that the pressure is constant across the boundary layer and the definition of the Chapman-Rubesin factor, C, to obtain

$$\delta^* \propto \frac{x}{\sqrt{Re_{1,x}}}\sqrt{C\left(\frac{T^*}{T_1}\right)^2 \frac{p_1}{p_e}} \propto \frac{x}{\sqrt{Re_{1,x}}} M_1^2 \sqrt{C}\sqrt{\frac{p_1}{p_e}}$$

Here we have assumed that μ varies linearly with T, and that $T^*/T_1 \propto M_1^2$.

Now, we can use the results from the hypersonic similarity parameter analysis of the oblique shock problem. Recall that we obtained an expression:

$$\frac{p_2}{p_1} = 1 + \frac{\gamma(\gamma+1)}{4}K^2 + \gamma K^2\sqrt{\Big(\frac{\gamma+1}{4}\Big)^2 + \frac{1}{K^2}} = \frac{p_e}{p_1}$$

Here the turning angle δ is given by the rate of change of the displacement thickness, $d\delta^*/dx$. Then

$$K = M_1\delta = M_1\frac{d\delta^*}{dx}$$

Consider two limits – the strong viscous interaction with $K^2 \gg 1$ and the weak interaction with $K^2 \ll 1$. For the strong interaction, we have

$$\frac{p_e}{p_1} \simeq \frac{\gamma(\gamma+1)}{2}K^2 = \frac{\gamma(\gamma+1)}{2}M_1^2\Big(\frac{d\delta^*}{dx}\Big)^2$$

And therefore, we have:

$$\delta^* \propto \frac{x}{\sqrt{Re_{1,x}}}M_1^2\sqrt{C}\frac{1}{M_1\big(d\delta^*/dx\big)}$$

$$\delta^*\, d\delta^* \propto \sqrt{\frac{\mu_1}{\rho_1 u_1}}M_1\sqrt{C}\sqrt{x}\, dx$$

This can be integrated to obtain:

$$\delta^* \propto x^{3/4}, \quad \frac{d\delta^*}{dx} \propto x^{-1/4}, \quad \frac{p_e}{p_1} \propto x^{-1/2}$$

Then,

$$K^2 = M_1^2\Big(\frac{d\delta^*}{dx}\Big)^2 \propto \frac{M_1^3}{\sqrt{Re_{1,x}}}\sqrt{C} = \bar{\chi}$$

Where $\bar{\chi}$ is the viscous interaction parameter. With this result, we can then write the pressure variation in the strong interaction regime as:

$$\frac{p_e}{p_1} = 1 + a_1\bar{\chi}$$

In the weak interaction regime, we assume that the boundary layer growth is not affected by the variation in the edge conditions, and we obtain

$$\frac{d\delta^*}{dx} \propto \frac{M_1^2}{\sqrt{Re_{1,x}}}\sqrt{C}$$

and therefore,

$$K = M_1\frac{d\delta^*}{dx} \propto \frac{M_1^3}{\sqrt{Re_{1,x}}}\sqrt{C} = \bar{\chi}$$

and

$$\frac{p_e}{p_1} = 1 + b_1\bar{\chi} + b_2\bar{\chi}^2$$

Hayes and Probstein used experimental data to fit the values of the constants. They obtained for an adiabatic wall flat plate:

$$\frac{p}{p_1} = 0.759 + 0.514\bar{\chi} \qquad \text{(Strong Interaction)}$$
$$\frac{p}{p_1} = 1 + 0.31\bar{\chi} + 0.05\bar{\chi}^2 \quad \text{(Weak Interaction)}$$

and for a cold wall ($T_w \ll T_{aw}$):

$$\frac{p}{p_1} = 1 + 0.15\bar{\chi} \qquad \text{(Strong Interaction)}$$
$$\frac{p}{p_1} = 1 + 0.078\bar{\chi} \qquad \text{(Weak Interaction)}$$

These comparisons show that when $\bar{\chi} > 3$, the strong interaction results should be used. Also note that $\bar{\chi}$ varies inversely with the square root of x, and therefore large $\bar{\chi}$ is near the leading edge.

Note that the pressure coefficient varies with the inverse of the free-stream Mach number squared. Therefore, the pressure coefficients and aerodynamic coefficients will scale with:

$$\frac{\bar{\chi}}{M_1^2} = \frac{M_1}{\sqrt{Re_{1,x}}}\sqrt{C} = \bar{V}$$

Generally, the L/D is reduced by viscous interactions, and high-lift vehicles are more adversely affected by viscous interactions than blunt capsule configurations.

Planetary Entry Dynamics

Now let us consider the dynamics of a hypersonic flight in the atmosphere. We will focus on planetary entry trajectories, but the equations of motion apply generally to high-speed flight in the atmosphere. Our emphasis will be on how the aerothermodynamics of the entry vehicle interplay with the trajectory flown. Thus to reduce the complexity of the analysis, we will make some simplifying approximations concerning the atmosphere and the entry trajectories.

Let us first consider the atmosphere and planetary properties. Let us assume:

1. The atmosphere and planet are spherical.
2. The variation of the atmospheric temperature and molecular weight are small relative to the variation of the density.
3. The peripheral speed of the planet is small compared to the entry speed. (Earth: satellite orbit period $\simeq$ 90 min, compared to 24 hour day.)

With these assumptions, we can determine the density variation and the characteristic low-orbit satellite speed. With hydrostatic equilibrium, we have:

$$dp = -\rho g \, dy$$

where y is the distance from the surface. With $p = \rho RT$ and the second assumption above, we have:

$$\begin{aligned} d\rho = \frac{\rho}{p} dp &= -\frac{1}{RT} \rho g \, dy \\ -\frac{1}{\rho} \frac{d\rho}{dy} &= \frac{g}{RT} = \beta \\ \rho &= \rho_o e^{-\beta y} \end{aligned}$$

where β is the inverse scale height, and is a property of the planet (mass, radius, and atmospheric composition, temperature). Note that with these assumptions, we have a direct mapping between altitude and density. Thus, we can work in terms of y or ρ in the analysis to follow.

Another important characteristic of a planet is its low-orbit satellite speed, V_s. This is the speed that a satellite would have if it were flying in equilibrium at "sea-level" altitude (the radius of curvature of its flight path is equal to the mean radius of the planet). In this case, we have:

$$\frac{mV_s^2}{R_o} = mg$$

where R_o is the planet radius, and g is the sea-level gravity. Thus,

$$V_s = \sqrt{gR_o}$$

which is a property of the planet. Table 1 gives some characteristic quantities for Earth, Venus, and Mars. We will see that planetary entry trajectories depend on these properties.

Table 1. Properties of Earth, Venus, and Mars.

Planet	R_o (km)	g (m/sec^2)	V_s (km/sec)	ρ_o (kg/m^3)	β (1/km)
Earth	6378	9.81	7.91	1.226	0.1378
Venus	6052	8.85	7.32	16.02	0.1606
Mars	3393	3.73	3.56	0.0993	0.0361

Equations of Motion for Planetary Entry

In this section, we derive the equations of motion for a spacecraft entering the atmosphere of a planet. The derivation relies on the following assumptions:

1. The planet is not rotating (or is rotating slowly relative to the entry time scale).
2. The entry occurs on a great circle; namely, the plane formed by the entry trajectory passes through the center of the planet.
3. The spacecraft behaves like a point mass.
4. The atmosphere has exponential density variation.
5. Ignore variation of g with altitude.

It is conventional to measure the flight path angle with γ, which is the angle relative to the local horizon (a spherical surface or radius equal to the planet radius plus the spacecraft altitude, centered at the planet center). Here, we will use the convention that a positive γ has the spacecraft entering the atmosphere; some analyses adopt the opposite convention.

Consider Fig. 18, which shows a two-dimensional representation of the trajectory plane. Here the inner circle represents the planetary surface, the outer circle is the local horizon, and r_c is the radius of curvature of the flight path. With the our convention, this example represents a case of positive flight path angle, γ.

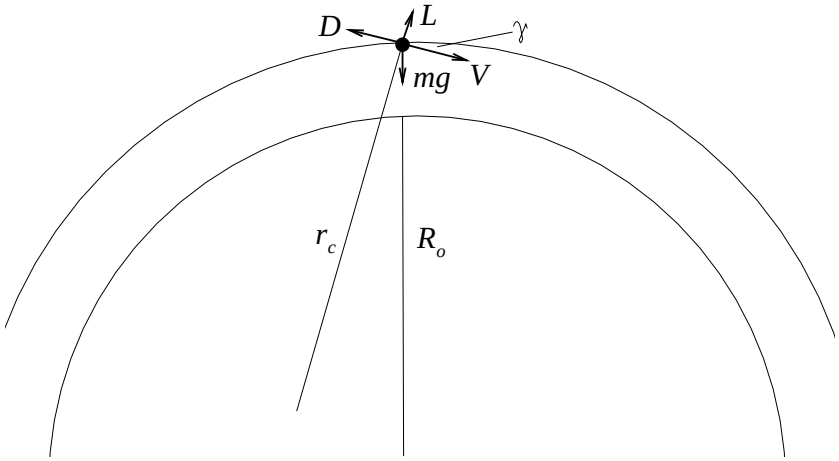

Figure 18. Free-body diagram of spacecraft during entry.

With this figure, it is easy to write the equations of motion; in the direction normal to flight path, we have:

$$L - mg\cos\gamma = -m\frac{V^2}{r_c}$$

and tangent to the flight path:

$$D - mg\sin\gamma = -m\frac{dV}{dt}$$

Now we must find an expression for r_c. The most straight-forward approach is to use a coordinate system in the normal and tangential directions (with unit vectors $\hat{e}_n$ and $\hat{e}_t$). Here, we let s be the distance along the flight path, and therefore the velocity and acceleration are given by:

$$\vec{V} = \dot{s}\hat{e}_t, \quad \vec{a} = \dot{\vec{V}} = \ddot{s}\hat{e}_t + \dot{s}\dot{\hat{e}}_t$$

where the dot represents the derivative with respect to time. Evaluating the acceleration is obvious, except for the derivative of the tangent unit vector.

It makes sense to derive $\dot{\hat{e}}_t$ in steps; first consider the case in which $\gamma = 0$ and it remains constant. In this case, we are flying at a constant altitude around the planet. Refering to Fig. 19, we can see that:

$$d\hat{e}_t = \hat{e}_t(t + \Delta t) - \hat{e}_t(t) = -d\theta\,\hat{e}_n$$

also, $R\,d\theta = V\,dt$, where R is the radius of the orbit, $R = R_o + y$. Therefore, we have the expected result:

$$\frac{d\hat{e}_t}{dt} = -\frac{V}{R}\,\hat{e}_n$$

It is easy to show that if γ is a non-zero constant, we have:

$$\frac{d\hat{e}_t}{dt} = -\frac{V}{R}\cos\gamma\,\hat{e}_n$$

Now, when γ is changing, there is an additional component added to $d\hat{e}_t$ due to $d\gamma$, as shown in Fig. 19. Then, we have:

$$\frac{d\hat{e}_t}{dt} = -\Big(\frac{V}{R}\cos\gamma + \frac{d\gamma}{dt}\Big)\hat{e}_n$$

Now, since $V = ds/dt$, we have:

$$\frac{d\gamma}{dt} = \frac{d\gamma}{ds}\frac{ds}{dt} = V\frac{d\gamma}{ds}$$

and the acceleration can be written as:

$$\vec{a} = \frac{dV}{dt}\hat{e}_t - V^2\Big(\frac{\cos\gamma}{R} + \frac{d\gamma}{ds}\Big)\hat{e}_n$$

Therefore, the local radius of curvature of the flight path is given by:

$$\frac{1}{r_c} = \frac{\cos\gamma}{R} + \frac{d\gamma}{ds}$$

where again, R is the distance to the center of the planet, $R = R_o + y$. It is also useful to note that:

$$dy = -\sin\gamma\,ds = -\frac{1}{\rho\beta}\,d\rho$$

Now we can derive an expression for the equation of motion in the flight-path normal direction:

$$L = \tfrac{1}{2}\rho V^2 C_L A = mg\cos\gamma - \frac{mV^2}{R}\cos\gamma - mV^2\frac{d\gamma}{ds}$$

Note that:

$$\frac{d\gamma}{ds} = -\sin\gamma\frac{d\gamma}{dy} = \frac{d(\cos\gamma)}{dy} = \beta\rho\frac{d(\cos\gamma)}{d\rho}$$

Then:

$$\frac{d(\cos\gamma)}{d\rho} = \frac{1}{2}\frac{L}{D}\frac{C_D A}{m}\frac{1}{\beta} - \frac{g}{\rho\beta}\frac{\cos\gamma}{V^2} + \frac{\cos\gamma}{\rho\beta R}$$

If we assume that $R \simeq R_o$, since for most planets the atmosphere is thin relative to the planet radius, we get:

$$\frac{d(\cos\gamma)}{d\rho} \simeq \frac{1}{2}\frac{L}{D}\frac{C_D A}{m}\frac{1}{\beta}\frac{\cos\gamma}{\rho\beta R_o}\Big(1 - \frac{V_s^2}{V^2}\Big)$$

Note that L/D and $m/C_D A$ are properties of the spacecraft, and β and V_s are properties of the planet. The quantity $m/C_D A$ is usually called the ballistic coefficient or ballistic parameter, and is often represented by B. (Some people represent $m/C_D A$ with β, which is easily confused with the inverse scale height.)

In a similar fashion, we can derive the equation of motion in the direction tangential to the flight path. One form of the resulting equation is:

$$\frac{d}{d\rho}\left(\frac{V^2}{V_s^2}\right) = \frac{1}{\rho}\frac{2}{\beta R_o} - \frac{C_D A}{m}\frac{1}{\beta}\frac{V^2}{V_s^2}\frac{1}{\sin\gamma}$$

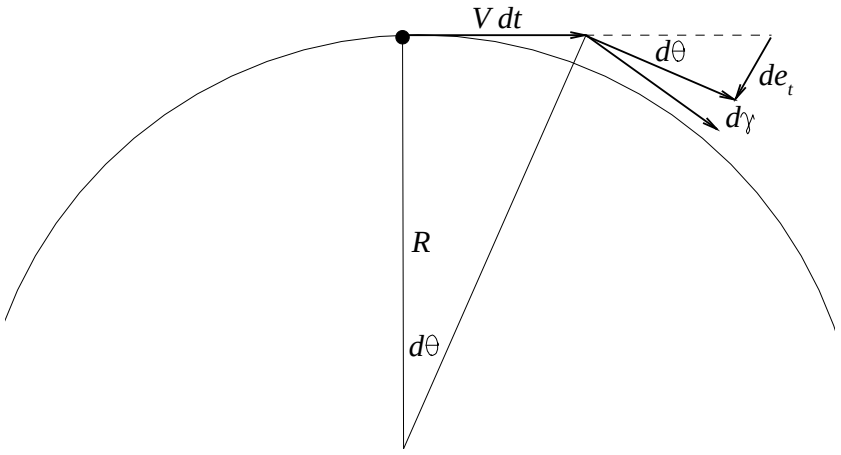

Figure 19. Variation of $\dot{\hat{e}}_t$ for constant altitude flight ($\gamma = 0$), and when $d\gamma \neq 0$.

Numerical Solution of Trajectory Equations of Motion

The equations of motion are usually written in a form similar to those given above. However, they have poor behavior when integrated numerically. For example, when $\sin\gamma$ approaches zero, the drag equation is singular. Also, $d\rho$ can be positive or negative, resulting in an ODE solver that must vary the sign of the incremented variable. Instead, we can derive a different form of the equations of motion:

$$\frac{d\gamma}{dt} = \frac{1}{V}\left[-\tfrac{1}{2}\rho V^2\frac{L}{D}\frac{1}{B} + g\cos\gamma - \frac{V^2}{R}\cos\gamma\right]$$
$$\frac{dV}{dt} = -\tfrac{1}{2}\rho V^2\frac{1}{B} + g\sin\gamma$$

These equations can be integrated in time much more easily than those presented earlier.

Shallow Lifting Glide Trajectory

In the case where γ is kept very small during the trajectory, the equations of motion may be simplified considerably. This is the shallow lifting glide or equilibrium glide trajectory, and is similar to what the Space Shuttle Orbiter flew. Here, we take γ to be constant

and very small; then from the lift equation, we have:

$$L = \tfrac{1}{2} C_L A \rho V^2 = mg - \frac{mV^2}{R_o}$$
$$\frac{R_o}{2}\frac{L}{D}\frac{1}{B}\rho V^2 = gR_o - V^2 = V_s^2 - V^2$$

and therefore:

$$\rho = \frac{2}{R_o}\frac{B}{L/D}\Big(\frac{V_s^2}{V^2} - 1\Big)$$

And since we know $\rho = \rho(y)$, we can determine flight speed as a function of altitude.

The range is determined from the drag equation:

$$D = -mV\frac{dV}{ds} = \tfrac{1}{2}\rho V^2 C_D A$$

Using the above expression for ρ, we obtain:

$$\big(V_s^2 - V^2\big)\frac{ds}{dV} = -R_o V \frac{L}{D}$$

which can be integrated to obtain:

$$\frac{V^2}{V_s^2} = 1 + \big(\frac{V_E^2}{V_s^2} - 1\Big)\exp\big(-\frac{2s}{R_o L/D}\big)$$

where s/R_o is the angular range measured along a great circle route from the point of entry (where $V = V_E$). It is also possible to compute the deceleration during and equilibrium glide trajectory.

Note that the equilibrium glide trajectory gives nonsense for $V_E > V_s$ unless $L/D < 0$. Thus, the vehicle would have to fly upside-down until $V < V_s$, at which point it would have to roll to change the direction of the lift vector.

In the above expression for ρ along the trajectory, notice that the term $\frac{B}{L/D}$ appears. This is important because B is proportional to the mass of the spacecraft; thus if L/D is increased, the spacecraft mass can be increased in proportion (assuming the other properties do not change). This is a major benefit from being able to fly a lifting trajectory.